Closed-Form 2-D Angle Estimation with Rectangular Arrays in Element Space or Beamspace via Unitary *ESPRIT*

Michael D. Zoltowski, *Senior Member, IEEE,* Martin Haardt, *Student Member,* and Cherian P. Mathews

***Abstract*— *UCA-ESPRIT* is a recently developed closed-form algorithm for use in conjunction with a uniform circular array (UCA) that provides automatically paired source azimuth and elevation angle estimates. *2-D unitary ESPRIT* is presented as an algorithm providing the same capabilities for a uniform rectangular array (URA). In the final stage of the algorithm, the real and imaginary parts of the ith eigenvalue of a matrix are one-to-one related to the respective direction cosines of the ith source relative to the two major array axes. *2-D unitary ESPRIT* offers a number of advantages over other recently proposed *ESPRIT* based closed-form 2-D angle estimation techniques. First, except for the final eigenvalue decomposition of dimension equal to the number of sources, it is efficiently formulated in terms of real-valued computation throughout. Second, it is amenable to efficient beamspace implementations that will be presented. Third, it is applicable to array configurations that do not exhibit identical subarrays, e. g., two orthogonal linear arrays. Finally, *2-D unitary ESPRIT* easily handles sources having one member of the spatial frequency coordinate pair in common. Simulation results are presented verifying the efficacy of the method.**

I. Introduction

For 1-D arrays, if the elements are uniformly spaced, *root-MUSIC* and *ESPRIT*[1] [1] avert a spectral search in determining the direction of arrival (DOA) of each incident signal. Instead, the DOA of each signal is determined from the roots of a polynomial. For either *root-MUSIC* or *ESPRIT*[2], the roots of interest ideally lie on the unit circle and are related one-to-one with each source as shown in Fig. 1.

For 2-D (planar) arrays, the fact that the fundamental theorem of algebra does not hold in two dimensions typically precludes a rooting type of formulation. Even for the highly regular uniform rectangular array (URA), *2-D MUSIC* requires a spectral search of a multimodal 2-D surface, while both *multiple invariance ESPRIT* [2], [3] and Clark and Scharf's *2-D IQML* [4] algorithm involve nonlinear optimization. Now, it should be pointed out that a URA lends itself to separable processing allowing one to decompose the 2-D problem into two 1-D problems. That is, one can estimate the DOA's with respect to one array axis via one set of calculations involving a *MUSIC*- or *ESPRIT*- based polynomial formulation, and do the same with respect to another array axis. Coupling information may be employed to subsequently pair the respective members of the two sets of 1-D angle estimates [5].

In the algebraically coupled matrix pencil (ACMP) method of van der Veen *et al.*,[3] eigenvector information is employed to pair the respective members of the two sets of 1-D angle estimates [6].

In contrast, for a uniform circular array (UCA) the recently developed *UCA-ESPRIT* [7], [8] algorithm provides closed-form, automatically paired 2-D angle estimates as long as the azimuth and elevation angle of each signal arrival is unique.

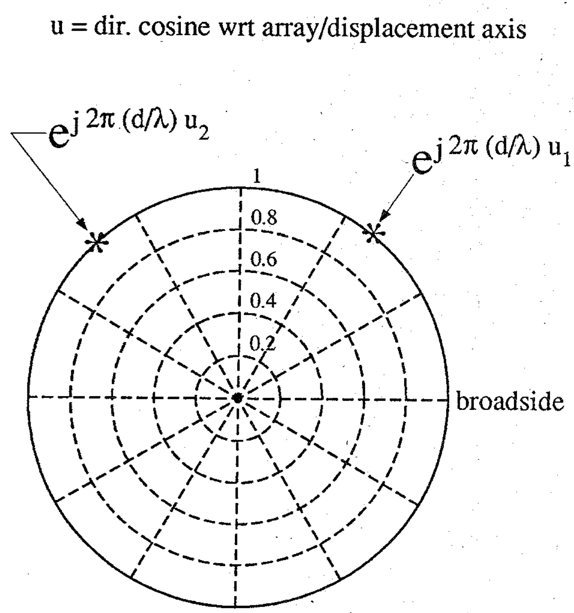

Fig. 1. Illustrating the form of signal roots obtained via root-MUSIC with ULA or ESPRIT with single invariance (roots are eigenvalues.)

Manuscript received July 11, 1994; revised July 24, 1995. This work was supported by AFOSR under contract no. F49620-95-1-0367 and by the National Science Foundation under grant no. MIP-9320890. The associate editor coordinating the review of this paper and approving it for publication was Dr. Geoffrey C. Orsak.

M. D. Zoltowski is with the School of Electrical Engineering, Purdue University, West Lafayette, IN 47907 USA (e-mail: mikedz@ecn.purdue.edu).

M. Haardt is with the Institute of Network Theory and Circuit Design, Technical University of Munich, Munich, Germany (e-mail: Martin.Haardt@nws.e-technik.tu-muenchen.de).

C. P. Mathews was with Purdue University, West Lafayette, IN 47907 USA. He is now with the Department of Electrical Engineering, University of West Florida, Pensacola, FL USA (e-mail: cmathews@uwf-uf.ee.uwf.edu).

Publisher Item Identifier S 1053-587X(96)01644-1.

[1] *ESPRIT* may also be employed in the case of an array composed of at least two translationally invariant subarrays.

[2] In *ESPRIT* the DOA's are extracted from eigenvalues, which are roots of the characteristic polynomial of a matrix.

[3] van der Veen *et al.* do not actually give their method a name. In a later paper, Vanpoucke *et al.* label their method ACMP.

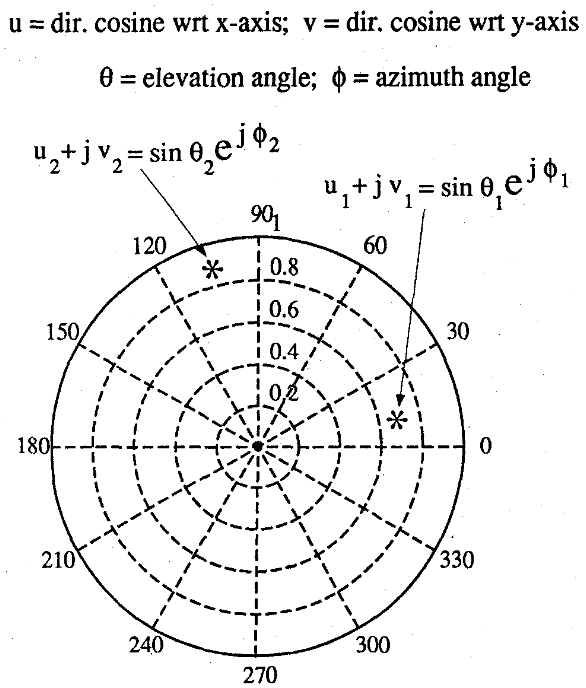

Fig. 2. Illustrating the form of signal roots obtained via UCA-ESPRIT with circular array or approximate 2-D DFT beamspace ESPRIT with rectangular array.

As illustrated in Fig. 2, in the final stage of *UCA-ESPRIT*, the ith eigenvalue of a matrix is of the form $\sin\theta_i\, e^{j\phi_i}$, where ϕ_i and θ_i are the azimuth and elevation angles of the ith source. Note that $\sin\theta_i\, e^{j\phi_i} = u_i + jv_i$ where u_i and v_i are the direction cosines of the ith source relative to the x and y axes, respectively. The eigenvalue for each source is thus unique such that *UCA-ESPRIT* does not have the aforementioned problem when two sources have the same u_i or the same v_i. We here develop a closed-form 2-D angle estimation algorithm for a URA that provides automatic pairing in a similar fashion. That is, in the final stage of new algorithm, referred to as *2-D unitary ESPRIT*, the real and imaginary parts of the ith eigenvalue of a matrix are one-to-one related to u_i and v_i, respectively.

2-D unitary ESPRIT is developed as an extension of the recently proposed *unitary ESPRIT* [9], [10] algorithm for a uniform linear array (ULA). *Unitary ESPRIT*exploits the conjugate centrosymmetry of the array manifold for a ULA to formulate each of the three primary stages of *ESPRIT* in terms of real-valued computations: 1) the computation of the signal eigenvectors; 2) the solution to the system of equations derived from these signal eigenvectors; and 3) the computation of the eigenvalues of the solution to the system of equations formed in stage 2. Note that Huarng & Yeh [11] and Linebarger *et al* [12] previously exploited the conjugate centrosymmetry of the ULA manifold to formulate the determination of the noise eigenvectors and subsequent spectral search required by *MUSIC* in terms of real-valued computation. The ability to formulate an *ESPRIT*-like algorithm for a ULA that only requires real-valued computations from start to finish, after an initial sparse unitary transformation, is critically important in developing a closed-form 2-D angle estimation algorithm for a URA similar to *UCA-ESPRIT* for a UCA. *unitary ESPRIT* is thus reviewed in Section III after a brief overview in Section II of $\mathcal{C}^N$ to $\Re^N$ transformations facilitated by the conjugate centro-symmetry of the ULA manifold.

A reduced dimension beamspace version of *unitary ESPRIT* is developed in Section IV. There are a number of advantages to working in beamspace: reduced computational complexity [13], decreased sensitivity to array imperfections [14], and lower signal-to-noise ratio (SNR) resolution thresholds [15]. In contrast to the *beamspace ESPRIT* [16] algorithm of Xu *et al*, the beamspace version of *unitary ESPRIT* exploits the real-valued nature of the beamspace manifold to formulate each of the three primary stages of *ESPRIT* in terms of real-valued computations as in *unitary ESPRIT*, but in a reduced dimension space. The relationship between *beamspace ESPRIT* and the beamspace version of *unitary ESPRIT* is examined in Section IV-B.

2-D unitary ESPRIT is developed in Section V. In addition to the ability to handle sources having the same arrival angle relative to either the x-axis or the y-axis, *2-D unitary ESPRIT*offers a number of advantages over other recently proposed *ESPRIT* based closed-form 2-D angle estimation techniques including ACMP. First, except for the final eigenvalue decomposition of dimension equal to the number of sources, it is efficiently formulated in terms of real-valued computation throughout. Second, it is amenable to a reduced dimension beamspace implementation. In Section VI, we develop a beamspace version of *2-D unitary ESPRIT* as an extension of the beamspace version of *unitary ESPRIT* presented in Section IV.

Another advantage of *2-D unitary ESPRIT* over ACMP is that the former is applicable to array configurations that do not exhibit identical 2-D subarrays, e. g., two noncollinear ULA's. In contrast, ACMP requires an array of sensor triplets so that one can extract three identical subarrays from the overall array. *2-D unitary ESPRIT* only requires that the array exhibit invariances in two distinct directions. In Section VII, we show how *2-D unitary ESPRIT* may be simply adapted for the case of two orthogonal ULA's having a common phase center. ACMP is not applicable with such an array geometry.

Simulation results are presented in Section VIII verifying the efficacy of *2-D unitary ESPRIT* and its beamspace counterpart, and comparing their respective performances with the Cramér–Rao lower bound.

II. Real-Valued Processing with a ULA

All of the developments in this paper rely on some well known aspects of real-valued processing with a ULA, which are quickly reviewed here [9]–[12], [17]. Employing the center of the ULA as the phase reference, the array manifold is conjugate centrosymmetric. For example, if the number of elements comprising the ULA N is odd, there is a sensor located at the array center and the array manifold is

$$\mathbf{a}_N(\mu) = \left[e^{-j\left(\frac{N-1}{2}\right)\mu}, \ldots, e^{-j\mu}, 1, e^{j\mu} \ldots, e^{j\left(\frac{N-1}{2}\right)\mu}\right]^T \quad (1)$$

where $\mu = \frac{2\pi}{\lambda}\Delta_x u$ with λ equal to the wavelength Δ_x is equal to the interelement spacing, and u equal to the direction cosine relative to the array axis. The conjugate centrosymmetry of $\mathbf{a}_N(\mu)$ is mathematically stated as $\mathbf{\Pi}_N \mathbf{a}_N(\mu) = \mathbf{a}_N^*(\mu)$ where

$$\mathbf{\Pi}_N = \begin{bmatrix} & & 1 \\ & 1 & \\ 1 & & \end{bmatrix} \in \Re^{N \times N}. \tag{2}$$

As the inner product between any two conjugate centrosymmetric vectors is real-valued, any matrix whose rows are each conjugate centrosymmetric may be employed to transform the complex-valued element space manifold $\mathbf{a}_N(\mu)$ into a real-valued manifold. As noted by numerous authors [9], [11], [12], the simplest matrices for accomplishing such are

$$\mathbf{Q}_{2K} = \frac{1}{\sqrt{2}} \begin{bmatrix} \mathbf{I}_K & j\,\mathbf{I}_K \\ \mathbf{\Pi}_K & -j\,\mathbf{\Pi}_K \end{bmatrix} \tag{3}$$

if N is even, or

$$\mathbf{Q}_{2K+1} = \frac{1}{\sqrt{2}} \begin{bmatrix} \mathbf{I}_K & \mathbf{0} & j\,\mathbf{I}_K \\ \mathbf{0}^T & \sqrt{2} & \mathbf{0}^T \\ \mathbf{\Pi}_K & \mathbf{0} & -j\,\mathbf{\Pi}_K \end{bmatrix} \tag{4}$$

if N is odd. $\mathbf{Q}_N^H$ is a sparse unitary matrix that transforms $\mathbf{a}_N(\mu)$ into an $N \times 1$ real-valued manifold, $\mathbf{d}_N(\mu) = \mathbf{Q}_N^H \mathbf{a}_N(\mu)$. For example, if the number of elements comprising the ULA is odd, the form in (4) is used and

$$\begin{aligned} \mathbf{d}_N(\mu) &= \mathbf{Q}_N^H \mathbf{a}_N(\mu) \\ &= \sqrt{2} \times \left[\cos\left(\frac{N\text{-}1}{2}\mu\right), \ldots, \cos(\mu), 1/\sqrt{2}, \right. \\ &\qquad \left. -\sin\left(\frac{N\text{-}1}{2}\mu\right), \ldots, -\sin(\mu)\right]^T. \end{aligned} \tag{5}$$

Let $\hat{\mathbf{R}}_{xx}$ denote the $N \times N$ complex-valued element space sample covariance matrix. Since the transformed manifold is real-valued, the signal eigenvectors required at the front end of *ESPRIT* may be computed as the "largest" eigenvectors of $\mathcal{R}e\{\mathbf{Q}_N^H \hat{\mathbf{R}}_{xx} \mathbf{Q}_N\}$. Note that in addition to the obvious computational reduction, taking the real part of the correlation matrix effects signal decorrelation [17] in the case of highly correlated or coherent sources. Alternatively, for robustness to dynamic range, if $\mathbf{X}$ denotes the $N \times N_s$ element space data matrix containing N_s snapshots as columns, the signal eigenvectors may be computed as the "largest" left singular vectors of the real-valued matrix $[\mathcal{R}e\{\mathbf{Y}\}, \mathcal{I}m\{\mathbf{Y}\}]$, where $\mathbf{Y} = \mathbf{Q}_N^H \mathbf{X}$.

Note that premultiplication of an $N \times 1$vector by $\mathbf{Q}_N^H$ involves no multiplications (the scaling by $\sqrt{2}$ is unnecessary in computing the signal eigenvectors) and only N additions. In Section IV, we also consider the use of the N-point DFT matrix, with appropriate scaling of the rows to make them each conjugate centrosymmetric [17] to transform the data into a real-valued beamspace. Although FFT's are fast, this approach ostensibly involves significantly more computation than the use of $\mathbf{Q}_N^H$. The utility of transforming to beamspace comes into play when there is *a priori* information on the general angular locations of the signal arrivals, as in a radar application, for example. In this case, one may only apply those rows of the DFT matrix that form beams encompassing the sector of interest. This yields a reduced dimension beamspace and leads to reduced computational complexity [13]–[15], [17].

Note that in this paper, we do not address the problem of estimating the number of sources. We will assume an estimate is available via a procedure such as that described by Xu *et al* in [18], which explicitly exploits the conjugate centrosymmetry of the array manifold for a ULA.

III. Review of Unitary Esprit for ULA

We here present a brief development of *unitary ESPRIT*as an alternative to that in [9] that provides further insight into *unitary ESPRIT* and also facilitates its extension for closed-form 2-D angle estimation scheme with a URA. We begin by developing an invariance relationship satisfied by the real-valued manifold $\mathbf{d}_N(\mu)$ in (5) that involves only real-valued quantities.

The element space manifold in (1) satisfies the invariance relation [1]

$$e^{j\mu}\mathbf{J}_1 \mathbf{a}_N(\mu) = \mathbf{J}_2 \mathbf{a}_N(\mu) \tag{6}$$

where $\mathbf{J}_1$ and $\mathbf{J}_2$ are the $(N-1) \times N$ selection matrices

$$\mathbf{J}_1 = \begin{bmatrix} 1 & 0 & 0 & \ldots & 0 & 0 \\ 0 & 1 & 0 & \ldots & 0 & 0 \\ \vdots & \vdots & \vdots & \ddots & \vdots & \vdots \\ 0 & 0 & 0 & \ldots & 1 & 0 \end{bmatrix} \in \Re^{(N-1)\times N} \tag{7}$$

$$\mathbf{J}_2 = \begin{bmatrix} 0 & 1 & 0 & \ldots & 0 & 0 \\ 0 & 0 & 1 & \ldots & 0 & 0 \\ \vdots & \vdots & \vdots & \ddots & \vdots & \vdots \\ 0 & 0 & 0 & \ldots & 0 & 1 \end{bmatrix} \in \Re^{(N-1)\times N}. \tag{8}$$

$\mathbf{J}_1$ and $\mathbf{J}_2$ select the first and last $N-1$ components of an $N \times 1$ vector, respectively. Since $\mathbf{Q}_N$ is unitary, it follows that $e^{j\mu}\mathbf{J}_1\mathbf{Q}_N\mathbf{Q}_N^H\mathbf{a}_N(\mu)$=$\mathbf{J}_2\mathbf{Q}_N\mathbf{Q}_N^H\mathbf{a}_N(\mu)$ which, invoking the definition of $\mathbf{d}_N(\mu)$ in (5), implies $e^{j\mu}\mathbf{J}_1\mathbf{Q}_N\mathbf{d}_N(\mu) = \mathbf{J}_2\mathbf{Q}_N\mathbf{d}_N(\mu)$. Premultiplying both sides by $\mathbf{Q}_{N-1}^H$ yields the following invariance relationship:

$$e^{j\mu}\mathbf{Q}_{N-1}^H\mathbf{J}_1\mathbf{Q}_N\mathbf{d}_N(\mu) = \mathbf{Q}_{N-1}^H\mathbf{J}_2\mathbf{Q}_N\mathbf{d}_N(\mu). \tag{9}$$

Note that $\mathbf{J}_1$ and $\mathbf{J}_2$ satisfy $\mathbf{\Pi}_{N\text{-}1}\mathbf{J}_2\mathbf{\Pi}_N = \mathbf{J}_1$. As a consequence,

$$\begin{aligned} \mathbf{Q}_{N-1}^H\mathbf{J}_2\mathbf{Q}_N &= \mathbf{Q}_{N-1}^H\mathbf{\Pi}_{N\text{-}1}\mathbf{\Pi}_{N\text{-}1}\mathbf{J}_2\mathbf{\Pi}_N\mathbf{\Pi}_N\mathbf{Q}_N \\ &= \mathbf{Q}_{N-1}^T\mathbf{J}_1\mathbf{Q}_N^* \\ &= (\mathbf{Q}_{N-1}^H\mathbf{J}_1\mathbf{Q}_N)^* \end{aligned} \tag{10}$$

where we have exploited the fact that $\mathbf{\Pi}_N\mathbf{Q}_N = \mathbf{Q}_N^*$ and $\mathbf{\Pi}_N\mathbf{\Pi}_N = \mathbf{I}_N$ for any N.

Let $\mathbf{K}_1$ and $\mathbf{K}_2$ be the real and imaginary parts of $\mathbf{Q}_{N-1}^H\mathbf{J}_2\mathbf{Q}_N$, as follows:

$$\mathbf{K}_1 = \mathcal{R}e\{\mathbf{Q}_{N-1}^H\mathbf{J}_2\mathbf{Q}_N\} \tag{11}$$

$$\mathbf{K}_2 = \mathcal{I}m\{\mathbf{Q}_{N-1}^H\mathbf{J}_2\mathbf{Q}_N\}. \tag{12}$$

$\mathbf{K}_1$ and $\mathbf{K}_2$ are real-valued $(N-1) \times N$ matrices. With these definitions, (9) may be expressed as

$$e^{j\frac{\mu}{2}}(\mathbf{K}_1 - j\mathbf{K}_2)\mathbf{d}_N(\mu) = e^{-j\frac{\mu}{2}}(\mathbf{K}_1 + j\mathbf{K}_2)\mathbf{d}_N(\mu). \tag{13}$$

Rearranging, we have

$$(e^{j\frac{\mu}{2}} - e^{-j\frac{\mu}{2}})\mathbf{K}_1\mathbf{d}_N(\mu) = j(e^{j\frac{\mu}{2}} + e^{-j\frac{\mu}{2}})\mathbf{K}_2\mathbf{d}_N(\mu). \tag{14}$$

Invoking the definition of the tangent function yields the following invariance relationship satisfied by $\mathbf{d}(\mu)$ involving only real-valued quantities:

$$\tan\left(\frac{\mu}{2}\right)\mathbf{K}_1\mathbf{d}_N(\mu)=\mathbf{K}_2\mathbf{d}_N(\mu). \quad (15)$$

For $d < N$ sources, we define the $N \times d$ real-valued DOA matrix as $\mathbf{D}=[\mathbf{d}_N(\mu_1),\mathbf{d}_N(\mu_2),...,\mathbf{d}_N(\mu_d)]$. The real-valued manifold relation in (15) translates into the real-valued DOA matrix relation

$$\mathbf{K}_1\mathbf{D}\boldsymbol{\Omega}_\mu=\mathbf{K}_2\mathbf{D},\ \text{ where:}\quad \boldsymbol{\Omega}_\mu=\text{diag}\left\{\tan\left(\frac{\mu_1}{2}\right),...,\tan\left(\frac{\mu_d}{2}\right)\right\}. \quad (16)$$

Now, as discussed previously, if $\mathbf{X}$ denotes the $N\times N_s$ element space data matrix containing N_s snapshots as columns, the signal eigenvectors for *unitary ESPRIT* may be computed as the "largest" left singular vectors of the real-valued matrix $[\mathcal{R}e\{\mathbf{Y}\},\mathcal{I}m\{\mathbf{Y}\}]$, where $\mathbf{Y}=\mathbf{Q}_N^H\mathbf{X}$. Asymptotically (i.e., as the number of snapshots becomes infinitely large), the $N\times d$ real-valued matrix of signal eigenvectors $\mathbf{E}_S$ is related to the real-valued $N \times d$ real-valued DOA matrix $\mathbf{D}$ as

$$\mathbf{E}_S=\mathbf{D}\mathbf{T} \quad (17)$$

where $\mathbf{T}$ is an unknown $d\times d$ *real-valued* matrix. Substituting $\mathbf{D}=\mathbf{E}_S\mathbf{T}^{-1}$ into (16) yields

$$\boldsymbol{\Gamma}_1\mathbf{E}_S\boldsymbol{\Psi}=\boldsymbol{\Gamma}_2\mathbf{E}_S,\quad \text{where:}\quad \boldsymbol{\Psi}=\mathbf{T}^{-1}\boldsymbol{\Omega}_\mu\mathbf{T}. \quad (18)$$

Thus, the eigenvalues of the $d\times d$ solution $\boldsymbol{\Psi}$ to the $(N-1)\times d$ matrix equation above are $\tan(\mu_i/2),\ i=1,...,d$. This reveals a spatial frequency warping identical to the temporal frequency warping incurred in designing a digital filter from an analog filter via the bilinear transformation. Consider $\Delta_x=\lambda/2$ so that $\mu=\frac{2\pi}{\lambda}\Delta_x u=\pi u$. In this case, there is a one-to-one mapping between $-1<u_i<1$, corresponding to the range of possible values for a direction cosine, and $-\infty<\omega_i<\infty$. *unitary ESPRIT* is summarized below.

Summary of unitary ESPRIT

1) Compute $\mathbf{E}_s$ via the d "largest" left singular vectors of $[\mathcal{R}e\{\mathbf{Y}\},\mathcal{I}m\{\mathbf{Y}\}]$, where $\mathbf{Y}=\mathbf{Q}_N^H\mathbf{X}$.
2) Compute $\boldsymbol{\Psi}$ as the solution to the $(N-1)\times d$ matrix equation $(\mathbf{K}_1\mathbf{E}_S)\boldsymbol{\Psi}=(\mathbf{K}_2\mathbf{E}_S)$.
3) Compute $\omega_i,\ i=1,...,d$, as the eigenvalues of the $d\times d$ real-valued matrix $\boldsymbol{\Psi}$.
4) Compute the spatial frequency estimates as $\mu_i=2\tan^{-1}(\omega_i),\ i=1,...,d$.

IV. DFT Beamspace *ESPRIT* for ULA

As an alternative to *unitary ESPRIT*, we here develop a version of *ESPRIT* for a ULA that works in DFT beamspace and involves only real-valued computation from start to finish after the initial transformation to beamspace. Reduced dimension processing in beamspace is facilitated when one has *apriori* information on the general angular locations of the signal arrivals, as in a radar application, for example. In this case, one may only apply those rows of the DFT matrix that form beams encompassing the sector of interest, thereby yielding reduced computational complexity. If there is no *a priori* information, one may examine the DFT spectrum and apply the algorithm to be developed to a small set of DFT values around each spectral peak above a particular threshold. In a more general setting, one may simply apply *DFT beamspace ESPRIT* via parallel processing to each of a number of sets of successive DFT values corresponding to overlapped sectors. Note, though, that in the development to follow, we will initially employ all N DFT beams for the sake of notational simplicity. A reduced dimension example will follow.

Applying the conjugate centrosymmetrized version of the m-th row of the N-point DFT matrix

$$\tilde{\mathbf{w}}_m^H=e^{j\left(\frac{N-1}{2}\right)m\frac{2\pi}{N}}\cdot\left[1\,,e^{-jm\frac{2\pi}{N}}\,,e^{-j2m\frac{2\pi}{N}}\,,\ldots\,,e^{-j(N-1)m\frac{2\pi}{N}}\right] \quad (19)$$

the mth component of the DFT beamspace manifold $0\le m\le(N-1)$ is

$$b_m(\mu)=\tilde{\mathbf{w}}_m^H\mathbf{a}_N(\mu)=\frac{\sin\left[\frac{N}{2}\left(\mu-m\frac{2\pi}{N}\right)\right]}{\sin\left[\frac{1}{2}\left(\mu-m\frac{2\pi}{N}\right)\right]}. \quad (20)$$

The row vector $\tilde{\mathbf{w}}_m^H$ represents a DFT beam steered at the spatial frequency $\mu^{(s)}=m\frac{2\pi}{N}$ (plus or minus integer multiples of 2π). Note that we can perform a front-end FFT (effectively implementing the Vandermonde form of the rows of the DFT matrix) and achieve conjugate symmetrized beamforming *a posteriori* through simple scaling of the DFT values (see (19)). The $N\times 1$ real-valued beamspace manifold is then

$$\mathbf{b}_N(\mu)=\tilde{\mathbf{W}}_N^H\mathbf{a}_N(\mu)=[b_0(\mu)\,,b_1(\mu)\,,\ldots\,,b_{N\text{-}1}(\mu)]^T \quad (21)$$

where $\tilde{\mathbf{W}}_N^H$ denotes the conjugate centrosymmetrized N pt. DFT matrix whose rows are given by (19).

Comparing $b_{m+1}(\mu)=\frac{\sin\left[\frac{N}{2}\left(\mu-(m+1)\frac{2\pi}{N}\right)\right]}{\sin\left[\frac{1}{2}\left(\mu-(m+1)\frac{2\pi}{N}\right)\right]}$ with $b_m(\mu)$ in (20), the numerator of $b_{m+1}(\mu)$ is observed to be the negative of that of $b_m(\mu)$. Thus, two successive components of the beamspace manifold are related as

$$\sin\left[\frac{1}{2}\left(\mu-m\frac{2\pi}{N}\right)\right]b_m(\mu)+\sin\left[\frac{1}{2}\left(\mu-(m{+}1)\frac{2\pi}{N}\right)\right]b_{m+1}(\mu)=0. \quad (22)$$

Trigonometric manipulations lead to

$$\tan\left(\frac{\mu}{2}\right)\left\{\cos\left(m\frac{\pi}{N}\right)b_m(\mu)+\cos\left((m+1)\frac{\pi}{N}\right)b_{m+1}(\mu)\right\}=\sin\left(m\frac{\pi}{N}\right)b_m(\mu)+\sin\left((m+1)\frac{\pi}{N}\right)b_{m+1}(\mu). \quad (23)$$

Hence, we could define two selection matrices of size $(N-1)\times N$ relating two successive components of the DFT beamspace manifold, namely $b_m(\mu)$ and $b_{m+1}(\mu)$, for $0\le m\le(N-2)$. Moreover, the beams with indices $m=(N-1)$ and $m=0$ are physically adjacent to one another, since they are steered at the spatial frequencies $\mu_{N-1}^{(s)}-2\pi=(N-1)\frac{2\pi}{N}-2\pi=-\frac{2\pi}{N}$ and $\mu_0^{(s)}=0$, respectively. To relate, therefore, the last and the first component the DFT beamspace manifold, i.e., $b_{N-1}(\mu)$ and $b_0(\mu)$ (see (21)), observe first that

$$\begin{aligned} b_N(\mu) &= \frac{\sin\left[\frac{N}{2}\left(\mu - N\frac{2\pi}{N}\right)\right]}{\sin\left[\frac{1}{2}\left(\mu - N\frac{2\pi}{N}\right)\right]} \\ &= \frac{\sin\left(\frac{N}{2}\mu - N\pi\right)}{\sin\left(\frac{1}{2}\mu - \pi\right)} \\ &= \frac{(-1)^N \cdot \sin\left(\frac{N}{2}\mu\right)}{-\sin\left(\frac{1}{2}\mu\right)} = (-1)^{(N-1)} \cdot b_0(\mu). \end{aligned}$$

Then, the desired relationship between $b_{N-1}(\mu)$ and $b_0(\mu)$ is obtained by setting $m = (N-1)$ in (23), namely

$$\tan\left(\frac{\mu}{2}\right)\left\{\cos\left((N-1)\frac{\pi}{N}\right)b_{N-1}(\mu) + \cos(\pi)(-1)^{(N-1)}b_0(\mu)\right\} = \sin\left((N-1)\frac{\pi}{N}\right)b_{N-1}(\mu) + \sin(\pi)(-1)^{(N-1)}b_0(\mu).$$

Compiling all N equations in vector form$0 \leq m \leq (N-1)$ yields an invariance relationship for the beamspace manifold $\mathbf{b}(\mu)$, similar to that for the real-valued manifold $\mathbf{d}_N(\mu)$, as follows:

$$\tan\left(\frac{\mu}{2}\right)\boldsymbol{\Gamma}_1\mathbf{b}_N(\mu) = \boldsymbol{\Gamma}_2\mathbf{b}_N(\mu) \tag{24}$$

where (25) and (26) are the result (see the bottom of the page).

Notice that the last rows of $\boldsymbol{\Gamma}_1$and $\boldsymbol{\Gamma}_2$ are a linear combination of the other rows, i.e., both $N \times N$ selection matrices are rank-deficient. They are only of rank $(N-1)$. One of the N rows of $\boldsymbol{\Gamma}_1$ and $\boldsymbol{\Gamma}_2$ could, therefore, be dropped, if all N DFT beams were employed. In reduced dimension processing, however, a subset of the row vectors defined in (19) is applied to the data matrix $\mathbf{X}$. Thus, only those subblocks of the selection matrices $\boldsymbol{\Gamma}_1$ and $\boldsymbol{\Gamma}_2$ that relate the corresponding components of $\mathbf{b}_N(\mu)$ will be used.

With d sources, the beamspace DOA matrix is $\mathbf{B} = [\mathbf{b}_N(\mu_1), \mathbf{b}_N(\mu_2), ..., \mathbf{b}_N(\mu_d)]$. The beamspace manifold relation in (24) translates into the beamspace DOA matrix relation

$$\begin{aligned} \boldsymbol{\Gamma}_1\mathbf{B}\boldsymbol{\Omega}_\mu = \boldsymbol{\Gamma}_2\mathbf{B}, \quad \text{where: } \boldsymbol{\Omega}_\mu \\ = \operatorname{diag}\left\{\tan\left(\frac{\mu_1}{2}\right), ..., \tan\left(\frac{\mu_d}{2}\right)\right\}. \end{aligned} \tag{27}$$

Now, the appropriate signal eigenvectors for the algorithm presently under development may be computed as the "largest" left singular vectors of the real-valued matrix $[\mathcal{Re}\{\mathbf{Y}\}, \mathcal{Im}\{\mathbf{Y}\}]$ where $\mathbf{Y} = \tilde{\mathbf{W}}_N^H\mathbf{X}$. Asymptotically, the $N \times d$ matrix of signal eigenvectors $\mathbf{E}_S$ satisfies $\mathbf{E}_S = \mathbf{BT}$, where $\mathbf{T}$ is an unknown $d \times d$ *real-valued* matrix. Substituting $\mathbf{B} = \mathbf{E}_S\mathbf{T}^{-1}$ into (27) yields

$$\boldsymbol{\Gamma}_1\mathbf{E}_S\boldsymbol{\Psi} = \boldsymbol{\Gamma}_2\mathbf{E}_S, \quad \text{where: } \boldsymbol{\Psi} = \mathbf{T}^{-1}\boldsymbol{\Omega}_\mu\mathbf{T}. \tag{28}$$

Thus, the eigenvalues of the $d \times d$ solution $\boldsymbol{\Psi}$ to the $(N-1) \times d$ matrix equation above are $\tan(\mu_i/2)$, $i = 1, ..., d$. The algorithm based on this development, *DFT beamspace ESPRIT*, is summarized below.

Summary of DFT beamspace ESPRIT

1) Compute $\mathbf{E}_s$ via the d "largest" left singular vectors of $[\mathcal{Re}\{\mathbf{Y}\}, \mathcal{Im}\{\mathbf{Y}\}]$ where $\mathbf{Y} = \tilde{\mathbf{W}}_N^H\mathbf{X}$.
2) Compute $\boldsymbol{\Psi}$ as the solution to the $(N-1) \times d$ matrix equation $(\boldsymbol{\Gamma}_1\mathbf{E}_S)\boldsymbol{\Psi} = (\boldsymbol{\Gamma}_2\mathbf{E}_S)$.
3) Compute ω_i, $i = 1, ..., d$, as the eigenvalues of the $d \times d$ real-valued matrix $\boldsymbol{\Psi}$.
4) Compute spatial frequency estimates as $\mu_i = 2\tan^{-1}(\omega_i)$, $i = 1, ..., d$.

A. Reduced Dimension Example

It is instructive to look at the structure of the selection matrices for *unitary ESPRIT*, $\mathbf{K}_1$ and $\mathbf{K}_2$ defined in (11) and (12), respectively. For example, for the case of $N = 6$ elements

$$\mathbf{K}_1 = \frac{1}{2}\begin{bmatrix} 1 & 1 & 0 & 0 & 0 & 0 \\ 0 & 1 & 1 & 0 & 0 & 0 \\ 0 & 0 & \sqrt{2} & 0 & 0 & 0 \\ 0 & 0 & 0 & 1 & 1 & 0 \\ 0 & 0 & 0 & 0 & 1 & 1 \end{bmatrix} \quad \text{and}$$

$$\mathbf{K}_2 = \frac{1}{2}\begin{bmatrix} 0 & 0 & 0 & -1 & 1 & 0 \\ 0 & 0 & 0 & 0 & -1 & 1 \\ 0 & 0 & 0 & 0 & 0 & -\sqrt{2} \\ 1 & -1 & 0 & 0 & 0 & 0 \\ 0 & 1 & -1 & 0 & 0 & 0 \end{bmatrix}.$$

Note that $\mathbf{K}_1$ and $\mathbf{K}_2$ are sparse like $\boldsymbol{\Gamma}_1$ and $\boldsymbol{\Gamma}_2$. However, any two rows of $\mathbf{K}_1$ and the corresponding rows of $\mathbf{K}_2$ involve all of the elements of $\mathbf{d}_N(\mu)$. (One needs two equations to

$$\boldsymbol{\Gamma}_1 = \begin{bmatrix} 1 & \cos\left(\frac{\pi}{N}\right) & 0 & 0 & \cdots & 0 & 0 \\ 0 & \cos\left(\frac{\pi}{N}\right) & \cos\left(\frac{2\pi}{N}\right) & 0 & \cdots & 0 & 0 \\ 0 & 0 & \cos\left(\frac{2\pi}{N}\right) & \cos\left(\frac{3\pi}{N}\right) & \cdots & 0 & 0 \\ \vdots & \vdots & \vdots & \vdots & \ddots & \vdots & \vdots \\ 0 & 0 & 0 & 0 & \cdots & \cos\left((N-2)\frac{\pi}{N}\right) & \cos\left((N-1)\frac{\pi}{N}\right) \\ (-1)^N & 0 & 0 & 0 & \cdots & 0 & \cos\left((N-1)\frac{\pi}{N}\right) \end{bmatrix} \in \Re^{N \times N} \tag{25}$$

$$\boldsymbol{\Gamma}_2 = \begin{bmatrix} 0 & \sin\left(\frac{\pi}{N}\right) & 0 & 0 & \cdots & 0 & 0 \\ 0 & \sin\left(\frac{\pi}{N}\right) & \sin\left(\frac{2\pi}{N}\right) & 0 & \cdots & 0 & 0 \\ 0 & 0 & \sin\left(\frac{2\pi}{N}\right) & \sin\left(\frac{3\pi}{N}\right) & \cdots & 0 & 0 \\ \vdots & \vdots & \vdots & \vdots & \ddots & \vdots & \vdots \\ 0 & 0 & 0 & 0 & \cdots & \sin\left((N-2)\frac{\pi}{N}\right) & \sin\left((N-1)\frac{\pi}{N}\right) \\ 0 & 0 & 0 & 0 & \cdots & 0 & \sin\left((N-1)\frac{\pi}{N}\right) \end{bmatrix} \in \Re^{N \times N} \tag{26}$$

estimate the DOA of one source.) Thus, one cannot work with a subset of the rows of $\mathbf{Q}_N^H$.

Again, the utility of *DFT beamspace ESPRIT* over *unitary ESPRIT* is in scenarios where one employs a subset of the rows of $\tilde{\mathbf{W}}_N^H$, the number of which depends on the width of the sector of interest and may be substantially less than N, to transform from element space to beamspace. Employing the appropriate subblocks of $\mathbf{\Gamma}_1$ and $\mathbf{\Gamma}_2$ as selection matrices, the algorithm is the same as that summarized previously except for the reduced dimensionality. For example, if one employed three successive rows of $\tilde{\mathbf{W}}_N^H$ associated with the DFT bin indices, m, $m+1$, and $m+2$, respectively, to form three beams in estimating the angles of two closely spaced signal arrivals, as in the low-angle radar tracking scheme described by Zoltowski and Lee [19], the appropriate 3×2 selection matrices are

$$\mathbf{\Gamma}_1 = \begin{bmatrix} \cos\left(m\frac{\pi}{N}\right) & \cos\left((m+1)\frac{\pi}{N}\right) & 0 \\ 0 & \cos\left((m+1)\frac{\pi}{N}\right) & \cos\left((m+2)\frac{\pi}{N}\right) \end{bmatrix}$$

and

$$\mathbf{\Gamma}_2 = \begin{bmatrix} \sin\left(m\frac{\pi}{N}\right) & \sin\left((m+1)\frac{\pi}{N}\right) & 0 \\ 0 & \sin\left((m+1)\frac{\pi}{N}\right) & \sin\left((m+2)\frac{\pi}{N}\right) \end{bmatrix}.$$

In this case, one would compute the $d = 2$ "largest" eigenvectors of a 3×3 real-valued matrix, solve a 2×2 real-valued system of equations, and compute the 2 eigenvalues of the resulting 2×2 matrix solution.

B. Relationship Between DFT Beamspace ESPRIT and Beamspace ESPRIT

In [16], Xu *et al.* develop a beamspace version of ESPRIT that is applicable whenever the $N_b \times N$ beamforming matrix $\mathbf{F}^H$ exhibits an invariance property similar to that exhibited by the element space DOA matrix in (6). Here N_b denotes the number of beams. That is, if $\mathbf{F}$ satisfies $\mathbf{J}_1\mathbf{F}\mathbf{\Theta} = \mathbf{J}_2\mathbf{F}$, where $\mathbf{\Theta}$ is an $N_b \times N_b$ diagonal matrix, then Xu *et al.* provide prescriptions for constructing $(N_b - 1) \times N_b$ matrices $\mathbf{\Sigma}_1$ and $\mathbf{\Sigma}_2$ satisfying $e^{j\mu}\mathbf{\Sigma}_1\mathbf{b}(\mu) = \mathbf{\Sigma}_2\mathbf{b}(\mu)$, where $\mathbf{b}(\mu)$ is the $N_b \times 1$ beamspace manifold $\mathbf{b}(\mu) = \mathbf{F}^H\mathbf{a}(\mu)$. This facilitates the use of ESPRIT in beamspace, ultimately yielding as eigenvalues the quantities $e^{j\mu_i}$, $i = 1, \ldots, d$ as in standard ESPRIT, except via processing in a reduced dimensional space.

Xu *et al* note that a beamforming matrix $\mathbf{F}^H$ composed of N_b rows of the N pt. DFT matrix satisfies a relationship of the form $\mathbf{J}_1\mathbf{F}\mathbf{\Theta} = \mathbf{J}_2\mathbf{F}$ thereby facilitating the use of *beamspace ESPRIT.* To see the relationship between *DFT beamspace ESPRIT* and *beamspace ESPRIT,* substitute the expression for $\tan(\mu/2)$ in (18) into the invariance relationship for $\mathbf{b}(\mu)$ in (24). After some manipulation this yields

$$(e^{j\mu} - 1)\mathbf{\Gamma}_1\mathbf{b}(\mu) = j(e^{j\mu} + 1)\mathbf{\Gamma}_2\mathbf{b}(\mu). \quad \Rightarrow$$
$$e^{j\mu}(\mathbf{\Gamma}_1 - j\mathbf{\Gamma}_2)\mathbf{b}(\mu) = (\mathbf{\Gamma}_1 + j\mathbf{\Gamma}_2)\mathbf{b}(\mu).$$

Thus, in this case the appropriate matrices $\mathbf{\Sigma}_1$ and $\mathbf{\Sigma}_2$ for *beamspace ESPRIT* are $\mathbf{\Sigma}_1 = \mathbf{\Gamma}_1 - j\mathbf{\Gamma}_2$ and $\mathbf{\Sigma}_2 = \mathbf{\Sigma}_1^*$. Note, though, that even if through centrosymmetrization one determines the signal eigenvectors via real-valued computation as discussed previously, the second and third stages of *beamspace ESPRIT* require complex-valued computation ultimately yielding as eigenvalues $e^{j\mu_i}$, $i = 1, \ldots, d$. Aside from the increased computation complexity relative to *DFT beamspace ESPRIT,* this does not facilitate an extension for the URA yielding automatically paired azimuth and elevation angle estimates.

V. 2-D Unitary Esprit for URA

We now develop an extension of *unitary ESPRIT* for a uniform rectangular array (URA) of $N \times M$ elements lying in the x-y plane and equispaced by Δ_x in the x direction and Δ_y in the y direction. In addition to $\mu = \frac{2\pi}{\lambda}\Delta_x u$, where u is the direction cosine variable relative to the x-axis, we define the spatial frequency variable $\nu = \frac{2\pi}{\lambda}\Delta_y v$, where v is the direction cosine variable relative to the y-axis.

In this development, in addition to representing the array manifold as an $NM \times 1$ vector, denoted $\mathbf{a}(\mu, \nu)$, it will be convenient to represent it as an $N \times M$ matrix denoted $\mathcal{A}(\mu, \nu)$, as well. The two forms are related through the operators $vec(\cdot)$ and $mat(\cdot)$ as $\mathbf{a}(\mu, \nu) = vec(\mathcal{A}(\mu, \nu))$ and $\mathcal{A}(\mu, \nu) = mat(\mathbf{a}(\mu, \nu))$. The operator $vec(\cdot)$ maps an $N \times M$ matrix to an $NM \times 1$ vector by stacking the columns of the matrix. The operator $mat(\cdot)$ performs the inverse mapping, mapping an $NM \times 1$ vector into an $N \times M$ matrix such that $mat(vec(\mathbf{X})) = \mathbf{X}$. An important property of the vec operator that will prove useful throughout the development is

$$vec(\mathbf{ABC}) = (\mathbf{C}^T \otimes \mathbf{A})\, vec(\mathbf{B}) \tag{29}$$

where $\otimes$ denotes the Kronecker matrix product.

In matrix form, the array manifold may be expressed as

$$\mathcal{A}(\mu, \nu) = \mathbf{a}_N(\mu)\mathbf{a}_M^T(\nu) \tag{30}$$

where $\mathbf{a}_M(\nu)$ is defined by (1) with N replaced by M and μ replaced by ν. Similar to the 1-D case, premultiplying $\mathcal{A}(\mu, \nu)$ by $\mathbf{Q}_N^H$ and post-multiplying by $\mathbf{Q}_M^*$, creates the $N \times M$ real-valued manifold

$$\begin{aligned} \mathcal{D}(\mu, \nu) &= \mathbf{Q}_N^H\mathcal{A}(\mu, \nu)\mathbf{Q}_M^* \\ &= \mathbf{Q}_N^H\mathbf{a}_N(\mu)\mathbf{a}_M^T(\nu)\mathbf{Q}_M^* \\ &= \mathbf{d}_N(\mu)\mathbf{d}_M^T(\nu) \end{aligned} \tag{31}$$

where $\mathbf{d}_M(\nu)$ is defined by (5) with N replaced by M and μ replaced by ν.

Given that $\mathbf{d}_N(\mu)$ satisfies the invariance relationship in (15), it follows that $\mathcal{D}(\mu, \nu)$ satisfies

$$\tan\left(\frac{\mu}{2}\right)\mathbf{K}_1\mathbf{D}(\mu, \nu) = \mathbf{K}_2\mathbf{D}(\mu, \nu) \tag{32}$$

where $\mathbf{K}_1$ and $\mathbf{K}_2$ are defined in (11) and (12), respectively. Using the property of the vec operator in (29), we find that the $NM \times 1$ real-valued manifold in vector form, $\mathbf{d}(\mu, \nu) = vec[\mathbf{D}(\mu, \nu)]$ satisfies

$$\tan\left(\frac{\mu}{2}\right)\mathbf{K}_{\mu 1}\mathbf{d}(\mu, \nu) = \mathbf{K}_{\mu 2}\mathbf{d}(\mu, \nu) \tag{33}$$

where $\mathbf{K}_{\mu 1}$ and $\mathbf{K}_{\mu 2}$ are the $(N-1)M \times NM$ matrices

$$\mathbf{K}_{\mu 1} = \mathbf{I}_M \otimes \mathbf{K}_1 \quad \text{and} \quad \mathbf{K}_{\mu 2} = \mathbf{I}_M \otimes \mathbf{K}_2. \tag{34}$$

Equation (33) represents $(N-1)M$ equations. Similarly, the 1-D real-valued manifold $\mathbf{d}_M(\nu)$ satisfies $\tan(\nu/2)$ $\cdot\mathbf{K}_3\mathbf{d}_M(\nu) = \mathbf{K}_4\mathbf{d}_M(\nu)$ where $\mathbf{K}_3$ and $\mathbf{K}_4$ are defined similar to (11) and (12) with N replaced by M such that they are $(M-1)\times M$. That is, $\mathbf{K}_3 = \mathcal{R}e\{\mathbf{Q}_{M-1}^H\mathbf{J}_2\mathbf{Q}_M\}$ and $\mathbf{K}_4 = \mathcal{I}m\{\mathbf{Q}_{M-1}^H\mathbf{J}_2\mathbf{Q}_M\}$. It follows that

$$\tan\left(\frac{\nu}{2}\right)\mathbf{D}(\mu,\nu)\mathbf{K}_3^T = \mathbf{D}(\mu,\nu)\mathbf{K}_4^T. \tag{35}$$

Again, using the vec operator, we find that $\mathbf{d}(\mu,\nu)$ satisfies

$$\tan\left(\frac{\nu}{2}\right)\mathbf{K}_{\nu 1}\mathbf{d}(\mu,\nu) = \mathbf{K}_{\nu 2}\mathbf{d}(\mu,\nu) \tag{36}$$

where $\mathbf{K}_{\nu 1}$f and $\mathbf{K}_{\nu 2}$ are the $N(M-1)\times NM$ matrices

$$\mathbf{K}_{\nu 1} = \mathbf{K}_3 \otimes \mathbf{I}_N \quad \text{and} \quad \mathbf{K}_{\nu 2} = \mathbf{K}_4 \otimes \mathbf{I}_N. \tag{37}$$

Equation (36) represents $N(M-1)$ equations.

Consider the $NM \times d$ real-valued DOA matrix $\mathbf{D} = [\mathbf{d}(\mu_1,\nu_1),\ldots,\mathbf{d}(\mu_d,\nu_d)]$, where $\mathbf{d}(\mu,\nu) = vec[\mathbf{D}(\mu,\nu)]$. (33) dictates that $\mathbf{D}$ satisfies

$$\mathbf{K}_{\mu 1}\mathbf{D}\mathbf{\Omega}_\mu = \mathbf{K}_{\mu 2}\mathbf{D} \tag{38}$$

where

$$\mathbf{\Omega}_\mu = \text{diag}\left\{\tan\left(\frac{\mu_1}{2}\right),\ldots,\tan\left(\frac{\mu_d}{2}\right)\right\}. \tag{39}$$

In turn, (36) dictates that $\mathbf{D}$ satisfies

$$\mathbf{K}_{\nu 1}\mathbf{D}\mathbf{\Omega}_\nu = \mathbf{K}_{\nu 2}\mathbf{D} \tag{40}$$

where

$$\mathbf{\Omega}_\nu = \text{diag}\left\{\tan\left(\frac{\nu_1}{2}\right),\ldots,\tan\left(\frac{\nu_d}{2}\right)\right\}. \tag{41}$$

Now, viewing the array output at a given snapshot as an $N\times M$ matrix, premultiply by $\mathbf{Q}_N^H$ and postmultiply by $\mathbf{Q}_M^*$, apply the vec operator and place the resulting $NM\times 1$ vector as a column of an $NM\times N_s$ data matrix $\mathbf{Y}$. Note that if $\mathbf{X}$ denotes the $NM\times N_s$ complex-valued element space data matrix, the relationship between $\mathbf{Y}$ and $\mathbf{X}$ may be expressed as $\mathbf{Y} = (\mathbf{Q}_M^H \otimes \mathbf{Q}_N^H)\mathbf{X}$ where we have again used the property of the vec operator in (29). The appropriate $NM\times d$ matrix of signal eigenvectors $\mathbf{E}_S$ for the algorithm presently under development may be computed as the d "largest" left singular vectors of the real-valued matrix $[\mathcal{R}e\{\mathbf{Y}\},\mathcal{I}m\{\mathbf{Y}\}]$. Asymptotically, $\mathbf{E}_S = \mathbf{DT}$ where $\mathbf{T}$ is an unknown $d\times d$ *real-valued* matrix. Substituting $\mathbf{D} = \mathbf{E}_S\mathbf{T}^{-1}$ into (38) and (40) yields the signal eigenvector relations

$$\mathbf{K}_{\mu 1}\mathbf{E}_S\mathbf{\Psi}_\mu = \mathbf{K}_{\mu 2}\mathbf{E}_S \quad \text{where:} \quad \mathbf{\Psi}_\mu = \mathbf{T}^{-1}\mathbf{\Omega}_\mu\mathbf{T} \tag{42}$$

$$\mathbf{K}_{\nu 1}\mathbf{E}_S\mathbf{\Psi}_\nu = \mathbf{K}_{\nu 2}\mathbf{E}_S \quad \text{where:} \quad \mathbf{\Psi}_\nu = \mathbf{T}^{-1}\mathbf{\Omega}_\nu\mathbf{T}. \tag{43}$$

Automatic pairing of μ and ν spatial frequency estimates is facilitated by the fact that all of the quantities in (42) and (43) are real valued. Thus, $\mathbf{\Psi}_\mu + j\mathbf{\Psi}_\nu$ may be spectrally decomposed as

$$\mathbf{\Psi}_\mu + j\mathbf{\Psi}_\nu = \mathbf{T}^{-1}\{\mathbf{\Omega}_\mu + j\mathbf{\Omega}_\nu\}\mathbf{T}. \tag{44}$$

The algorithm based on this development, *2-D unitary ESPRIT*, is summarized below.

Summary of 2-D unitary ESPRIT

1) Compute $\mathbf{E}_s$ via d "largest" left singular vectors of $[\mathcal{R}e\{\mathbf{Y}\},\mathcal{I}m\{\mathbf{Y}\}]$ where $\mathbf{Y} = (\mathbf{Q}_M^H \otimes \mathbf{Q}_N^H)\mathbf{X}$.

2a) Compute $\mathbf{\Psi}_\mu$ as the solution to the $(N-1)M\times d$ matrix equation $\mathbf{K}_{\mu 1}\mathbf{E}_S\mathbf{\Psi}_\mu = \mathbf{K}_{\mu 2}\mathbf{E}_S$.

2b) Compute $\mathbf{\Psi}_\nu$ as the solution to the $N(M-1)\times d$ matrix equation $\mathbf{K}_{\nu 1}\mathbf{E}_S\mathbf{\Psi}_\nu = \mathbf{K}_{\nu 2}\mathbf{E}_S$.

3) Compute λ_i, $i = 1,\ldots,d$, as the eigenvalues of the $d\times d$ matrix $\mathbf{\Psi}_\mu + j\mathbf{\Psi}_\nu$.

4) Compute spatial frequency estimates $\mu_i = 2\tan^{-1}(\mathcal{R}e\{\lambda_i\})$, $\nu_i = 2\tan^{-1}(\mathcal{I}m\{\lambda_i\})$, $i = 1,\cdots,d$

Note that the maximum number of sources *2-D unitary ESPRIT* can handle is minimum$\{M(N-1), N(M-1)\}$, assuming that at least $d/2$ snapshots are available (we are inherently effecting a forward-backward average that effectively doubles the number of snapshots.) If only a single snapshot is available, one can extract $d/2$ or more identical rectangular subarrays out of the overall array to get the effect of multiple snapshots, thereby decreasing the maximum number of sources that can be handled.

Note that *2-D unitary ESPRIT* provides closed-form, automatically paired 2-D angle estimates as long as the spatial frequency coordinate pairs $(\mu_i,\nu_i), i = 1,\ldots,d$ are distinct. That is, no additional effort is needed if a pair or more of sources have the same μ_i or ν_i. Note that in order to avoid the same problem as ACMP in this regard, one must solve the complex eigenvalue problem signified by (44). If one attempts to compute the real eigenvalues of $\mathbf{\Psi}_\mu$ alone, for example, there is a degeneracy in the eigenvectors when two sources have the same μ spatial frequency coordinate thereby precluding the ability to determine $\mathbf{T}$.

VI. 2-D DFT Beamspace ESPRIT for URA

With 2-D DFT beamforming (and attendant conjugate centrosymmetrization through simple scaling), the components of the beamspace array manifold are separable real-valued patterns of the form

$$b_{m,n}(\mu,\nu) = \frac{\sin\left[\frac{N}{2}\left(\mu - m\frac{2\pi}{N}\right)\right]}{\sin\left[\frac{1}{2}\left(\mu - m\frac{2\pi}{N}\right)\right]}\,\frac{\sin\left[\frac{M}{2}\left(\nu - n\frac{2\pi}{M}\right)\right]}{\sin\left[\frac{1}{2}\left(\nu - n\frac{2\pi}{M}\right)\right]}. \tag{45}$$

Note that the matrix form of the beamspace manifold, denoted $\mathcal{B}(\mu,\nu)$, is related to the matrix form of the array manifold via a 2-D DFT as $\mathcal{B}(\mu,\nu) = \tilde{\mathbf{W}}_N^H\mathcal{A}(\mu,\nu)\tilde{\mathbf{W}}_M^*$ where $\tilde{\mathbf{W}}_N^H$ denotes the conjugate centrosymmetrized N-point DFT matrix whose rows are given by (19) and $\tilde{\mathbf{W}}_M^H$ is defined similarly with N replaced by M. Substituting the form of $\mathcal{A}(\mu,\nu)$ in (30) into $\mathcal{B}(\mu,\nu) = \tilde{\mathbf{W}}_N^H\mathcal{A}(\mu,\nu)\tilde{\mathbf{W}}_M^*$ yields

$$\mathcal{B}(\mu,\nu) = \mathbf{b}_N(\mu)\mathbf{b}_M^T(\nu) \tag{46}$$

where $\mathbf{b}_N(\mu)$ is defined in (21) and $\mathbf{b}_M(\nu)$ is defined similarly with N replaced by M and μ replaced by ν. Given that $\mathbf{b}_N(\mu)$ satisfies the invariance relationship in (24), it follows that $\mathcal{B}(\mu,\nu)$ satisfies

$$\tan\left(\frac{\mu}{2}\right)\mathbf{\Gamma}_1\mathbf{B}(\mu,\nu) = \mathbf{\Gamma}_2\mathbf{B}(\mu,\nu). \tag{47}$$

where $\mathbf{\Gamma}_1$ and $\mathbf{\Gamma}_2$ are defined in (25) and (26). Using the property of the vec operator in (29), we find that the $NM\times 1$ beamspace manifold in vector form $\mathbf{b}(\mu,\nu) = vec[\mathbf{B}(\mu,\nu)]$ satisfies

$$\tan\left(\frac{\mu}{2}\right)\mathbf{\Gamma}_{\mu 1}\mathbf{b}(\mu,\nu) = \mathbf{\Gamma}_{\mu 2}\mathbf{b}(\mu,\nu), \tag{48}$$

where $\boldsymbol{\Gamma}_{\mu 1}$ and $\boldsymbol{\Gamma}_{\mu 2}$ are the $(N-1)M \times NM$ matrices:

$$\boldsymbol{\Gamma}_{\mu 1} = \mathbf{I}_M \otimes \boldsymbol{\Gamma}_1 \quad \text{and} \quad \boldsymbol{\Gamma}_{\mu 2} = \mathbf{I}_M \otimes \boldsymbol{\Gamma}_2. \tag{49}$$

Equation (48) represents $(N-1)M$ equations obtained by comparing each pair of adjacent beams having the same μ pointing angle coordinate. Similarly, the 1-D beamspace manifold $\mathbf{b}_M(\nu)$ satisfies $\tan(\nu/2)\ \boldsymbol{\Gamma}_3\mathbf{b}_M(\nu) = \boldsymbol{\Gamma}_4\mathbf{b}_M(\nu)$ where $\boldsymbol{\Gamma}_3$ and $\boldsymbol{\Gamma}_4$ are defined similar to (25) and (26) with N replaced by M such that they are $(M-1)\times M$. It follows that

$$\tan\left(\frac{\nu}{2}\right)\mathbf{B}(\mu,\nu)\boldsymbol{\Gamma}_3^T = \mathbf{B}(\mu,\nu)\boldsymbol{\Gamma}_4^T. \tag{50}$$

Again, using the *vec* operator, we find that $\mathbf{b}(\mu,\nu)$ satisfies

$$\tan\left(\frac{\nu}{2}\right)\boldsymbol{\Gamma}_{\nu 1}\mathbf{b}(\mu,\nu) = \boldsymbol{\Gamma}_{\nu 2}\mathbf{b}(\mu,\nu) \tag{51}$$

where $\boldsymbol{\Gamma}_{\nu 1}$ and $\boldsymbol{\Gamma}_{\nu 2}$ are the $N(M-1)\times NM$ matrices as follows:

$$\boldsymbol{\Gamma}_{\nu 1} = \boldsymbol{\Gamma}_3 \otimes \mathbf{I}_N \quad \text{and} \quad \boldsymbol{\Gamma}_{\nu 2} = \boldsymbol{\Gamma}_4 \otimes \mathbf{I}_N. \tag{52}$$

Equation (51) represents $N(M-1)$ equations obtained by comparing each pair of adjacent beams having the same ν pointing angle coordinate.

Consider the $NM \times d$ real-valued beamspace DOA matrix $\mathbf{B} = [\mathbf{b}(\mu_1,\nu_1),\ldots,\mathbf{b}(\mu_d,\nu_d)]$. (48) dictates that $\mathbf{B}$ satisfies

$$\boldsymbol{\Gamma}_{\mu 1}\mathbf{B}\boldsymbol{\Omega}_\mu = \boldsymbol{\Gamma}_{\mu 2}\mathbf{B} \tag{53}$$

where $\boldsymbol{\Omega}_\mu$ is defined in (39). In turn, (51) dictates that $\mathbf{B}$ satisfies

$$\boldsymbol{\Gamma}_{\nu 1}\mathbf{B}\boldsymbol{\Omega}_\nu = \boldsymbol{\Gamma}_{\nu 2}\mathbf{B} \tag{54}$$

where $\boldsymbol{\Omega}_\nu$ is defined in (41).

Now, viewing the array output at a given snapshot as an $N \times M$ matrix, we compute a 2-D DFT, apply the *vec* operator, and place the resulting $NM \times 1$ vector as a column of an $NM \times N_s$ data matrix $\mathbf{Y}$. Recall that $\mathbf{X}$ denotes the $NM \times N_s$ data matrix prior to the 2-D DFT. Using the *vec* operator, the relationship between $\mathbf{Y}$ and $\mathbf{X}$ may be expressed as $\mathbf{Y} = (\tilde{\mathbf{W}}_M^H \otimes \tilde{\mathbf{W}}_N^H)\mathbf{X}$. The appropriate $NM \times d$ matrix of signal eigenvectors, $\mathbf{E}_S$, for the algorithm presently under development may be computed as the d "largest" left singular vectors of the real-valued matrix $[\mathcal{R}e\{\mathbf{Y}\}, \mathcal{I}m\{\mathbf{Y}\}]$. Asymptotically, $\mathbf{E}_S = \mathbf{BT}$, where $\mathbf{T}$ is an unknown $d \times d$ *real-valued* matrix. Substituting $\mathbf{B} = \mathbf{E}_S\mathbf{T}^{-1}$ into (53) and (54) yields the signal eigenvector relations

$$\boldsymbol{\Gamma}_{\mu 1}\mathbf{E}_S\boldsymbol{\Psi}_\mu = \boldsymbol{\Gamma}_{\mu 2}\mathbf{E}_S \quad \text{where:} \quad \boldsymbol{\Psi}_\mu = \mathbf{T}^{-1}\boldsymbol{\Omega}_\mu\mathbf{T} \tag{55}$$

$$\boldsymbol{\Gamma}_{\nu 1}\mathbf{E}_S\boldsymbol{\Psi}_\nu = \boldsymbol{\Gamma}_{\nu 2}\mathbf{E}_S \quad \text{where:} \quad \boldsymbol{\Psi}_\nu = \mathbf{T}^{-1}\boldsymbol{\Omega}_\nu\mathbf{T}. \tag{56}$$

As in the extension of *unitary ESPRIT* for a URA, automatic pairing of μ and ν spatial frequency estimates is facilitated by the fact that all of the quantities in (55) and (56) are real valued. Thus, $\boldsymbol{\Psi}_\mu + j\boldsymbol{\Psi}_\nu$ may be spectrally decomposed as $\boldsymbol{\Psi}_\mu + j\boldsymbol{\Psi}_\nu = \mathbf{T}^{-1}\{\boldsymbol{\Omega}_\mu + j\boldsymbol{\Omega}_\nu\}\mathbf{T}$. The algorithm based on this development, *2-D DFT beamspace ESPRIT*, is summarized below.

Summary of 2-D DFT beamspace ESPRIT

1) Compute a 2-D DFT of the $N \times M$ matrix of array outputs at each snapshot (scale for conjugate centrosymmetrization), apply the *vec* operator, and place the result as a column of $\mathbf{Y}$.
2) Compute $\mathbf{E}_s$ via the d "largest" left singular vectors of $[\mathcal{R}e\{\mathbf{Y}\}, \mathcal{I}m\{\mathbf{Y}\}]$.

3a) Compute $\boldsymbol{\Psi}_\mu$ as the solution to the $(N-1)M \times d$ matrix equation $\boldsymbol{\Gamma}_{\mu 1}\mathbf{E}_S\boldsymbol{\Psi}_\mu = \boldsymbol{\Gamma}_{\mu 2}\mathbf{E}_S$.

3b) Compute $\boldsymbol{\Psi}_\nu$ as the solution to the $N(M-1) \times d$ matrix equation $\boldsymbol{\Gamma}_{\nu 1}\mathbf{E}_S\boldsymbol{\Psi}_\nu = \boldsymbol{\Gamma}_{\nu 2}\mathbf{E}_S$.

4) Compute λ_i, $i = 1,\ldots,d$, as the eigenvalues of the $d \times d$ matrix $\boldsymbol{\Psi}_\mu + j\boldsymbol{\Psi}_\nu$.
5) Compute spatial frequency estimates $\mu_i = 2\tan^{-1}(\mathcal{R}e\{\lambda_i\})$, $\nu_i = 2\tan^{-1}(\mathcal{I}m\{\lambda_i\})$, $i = 1,\ldots,d$.

A. Reduced Dimension Example

As in the 1-D case, the utility of *2-D DFT beamspace ESPRIT* over *2-D unitary ESPRIT* is in scenarios where one works with a subset of 2-D DFT beams that encompass some volume of space of interest. In fact, the ability to work in a reduced dimension beamspace is even of more value in the case of a URA since the total number of elements may be quite high. As an example, consider a scenario, similar to the low-angle radar tracking problem, in which we wish to estimate the respective azimuth and elevation angles of each of two closely spaced sources. To this end, we form four 2-D DFT beams steered to the spatial frequency coordinate pairs $(m\frac{2\pi}{N}, n\frac{2\pi}{M})$, $((m+1)\frac{2\pi}{N}, n\frac{2\pi}{M})$, $(m\frac{2\pi}{N}, (n+1)\frac{2\pi}{M})$, and $((m+1)\frac{2\pi}{N}, (n+1)\frac{2\pi}{M})$, respectively, as depicted in Fig. 3. Recalling that the components of the beamspace manifold have the form in (45), the 4×1 beamspace manifold for this case is

$$\mathbf{b}(\mu,\nu) = [b_{m,n}(\mu,\nu), b_{m+1,n}(\mu,\nu), b_{m,n+1}(\mu,\nu), b_{m+1,n+1}(\mu,\nu)]^T. \tag{57}$$

In this case, $\mathbf{E}_S$ is 4×2 and may be constructed from the two "largest" eigenvectors of the real part of the 4×4 matrix formed from the interbeam correlations. The 2×2 matrices $\boldsymbol{\Psi}_\mu$ and $\boldsymbol{\Psi}_\nu$ would be computed as the corresponding solutions to the 2×2 respective matrix equations $\boldsymbol{\Gamma}_{\mu 1}\mathbf{E}_S\boldsymbol{\Psi}_\mu = \boldsymbol{\Gamma}_{\mu 2}\mathbf{E}_S$ and $\boldsymbol{\Gamma}_{\nu 1}\mathbf{E}_S\boldsymbol{\Psi}_\nu = \boldsymbol{\Gamma}_{\nu 2}\mathbf{E}_S$, where

$$\boldsymbol{\Gamma}_{\mu 1} = \begin{bmatrix} \cos\left(m\frac{\pi}{N}\right) & 0 & \cos\left((m+1)\frac{\pi}{N}\right) & 0 \\ 0 & \cos\left(m\frac{\pi}{N}\right) & 0 & \cos\left((m+1)\frac{\pi}{N}\right) \end{bmatrix}$$

$$\boldsymbol{\Gamma}_{\mu 2} = \begin{bmatrix} \sin\left(m\frac{\pi}{N}\right) & 0 & \sin\left((m+1)\frac{\pi}{N}\right) & 0 \\ 0 & \sin\left(m\frac{\pi}{N}\right) & 0 & \sin\left((m+1)\frac{\pi}{N}\right) \end{bmatrix}$$

$$\boldsymbol{\Gamma}_{\nu 1} = \begin{bmatrix} \cos\left(n\frac{\pi}{M}\right) & 0 & \cos\left((n+1)\frac{\pi}{M}\right) & 0 \\ 0 & \cos\left(n\frac{\pi}{M}\right) & 0 & \cos\left((n+1)\frac{\pi}{M}\right) \end{bmatrix}$$

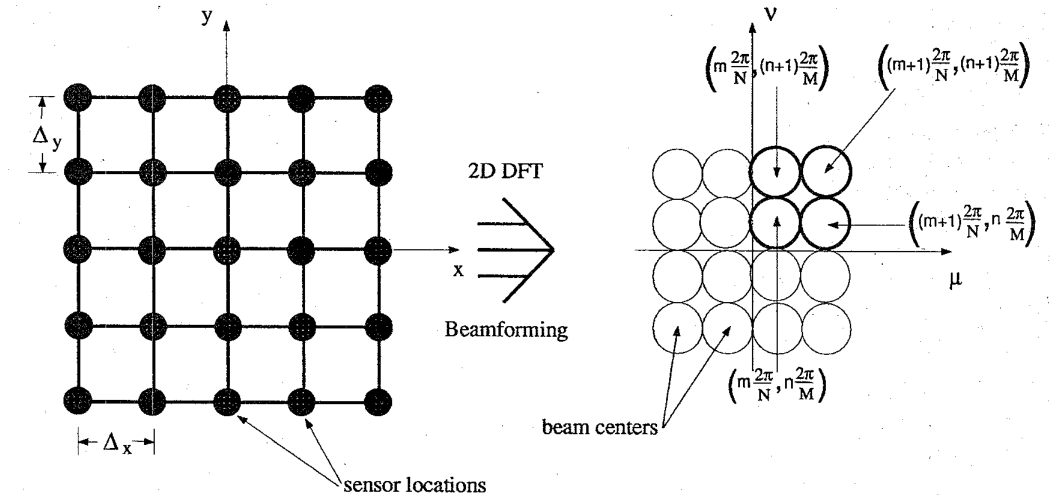

Fig. 3. Illustration of transformation from element space to beamspace, highlighting four-beam example for 2-D DFT beamspace ESPRIT.

$$\boldsymbol{\Gamma}_{\nu 2} = \begin{bmatrix} \sin\left(n\frac{\pi}{M}\right) & 0 & \sin\left((n+1)\frac{\pi}{M}\right) & 0 \\ 0 & \sin\left(n\frac{\pi}{M}\right) & 0 & \sin\left((n+1)\frac{\pi}{M}\right) \end{bmatrix}.$$

In the final stage of the algorithm $\tan(\mu_i/2) + j\tan(\nu_i/2)$, $i = 1, 2$ would be computed as the eigenvalues of a 2×2 matrix.

B. Comparison with UCA-ESPRIT

As discussed in Section I, *UCA-ESPRIT* [7], [8] is a recently developed closed-form 2-D angle estimation scheme for a UCA. As indicated in Fig. 2, in the final stage of *UCA-ESPRIT*, the i-th eigenvalue of a matrix has the form $u_i + jv_i$, where u_i and v_i are the direction cosines of the ith source relative to the x and y axes, respectively, assuming the UCA to lie in the x-y plane. This is in contrast to *2-D DFT beamspace ESPRIT* where there is spatial frequency warping such that the final eigenvalues are of the form $\tan(\mu_i/2) + j\tan(\nu_i/2)$, $i = 1, \ldots, d$. A notable difference between the development of *UCA-ESPRIT* and that of *2-D DFT beamspace ESPRIT* is that in the former the sampled aperture pattern was assumed to be approximately equal to the continuous aperture pattern [7], [8] while no such approximation was made in the latter case. We here briefly show that if a similar approximation is made in the development of *2-D DFT beamspace ESPRIT*, the final eigenvalues yielded by the resulting approximate *2-D DFT beamspace ESPRIT* algorithm are identical in form to those yielded by *UCA-ESPRIT*.

Aside from averting spatial frequency warping, this form of the eigenvalue has a nice geometrical interpretation in that it may be expressed as $u_i + jv_i = \sin\theta_i\, e^{j\phi_i}$ where ϕ_i and θ_i are the azimuth and elevation angles of the ith source, respectively. This is illustrated in Fig. 2. θ_i varies between 0° and 90° so that $\sin\theta_i$ varies between 0 and 1, while ϕ_i varies between 0° and 360°. Thus, one can immediately glean the azimuth angle of the ith source from the polar angle of the ith eigenvalue. The corresponding elevation angle is the arcsine of the magnitude of the$i$th eigenvalue. If the eigenvalue is at the origin, the source is at boresite. If the eigenvalue is on the unit circle, the source is in the same plane as the array. Also, we may use the fact that an eigenvalue should be located on or within the unit circle to screen out false alarms.

Assume the interelement spacing in either direction to be less than or equal to a half-wavelength. In this case, in the vicinity of the mainlobe and first few sidelobes, $b_{m,n}(\mu,\nu) \approx \frac{\sin\left[\frac{N}{2}\left(\mu - m\frac{2\pi}{N}\right)\right]}{\frac{1}{2}\left(\mu - m\frac{2\pi}{N}\right)} \frac{\sin\left[\frac{M}{2}\left(\nu - n\frac{2\pi}{M}\right)\right]}{\frac{1}{2}\left(\nu - n\frac{2\pi}{M}\right)}$. Substituting $\mu = \frac{2\pi}{\lambda}\Delta_x u$ and $\nu = \frac{2\pi}{\lambda}\Delta_y v$, define

$$b^a_{m,n}(u,v) = \frac{\sin\left[\frac{N}{2}\left(\frac{2\pi}{\lambda}\Delta_x u - m\frac{2\pi}{N}\right)\right]}{\frac{1}{2}\left(\frac{2\pi}{\lambda}\Delta_x u - m\frac{2\pi}{N}\right)} \cdot \frac{\sin\left[\frac{M}{2}\left(\frac{2\pi}{\lambda}\Delta_y v - n\frac{2\pi}{M}\right)\right]}{\frac{1}{2}\left(\frac{2\pi}{\lambda}\Delta_y v - n\frac{2\pi}{M}\right)}. \tag{58}$$

This is the far-field pattern that would result with a continuous rectangular aperture of dimension $N\Delta_x$ by $M\Delta_y$. The superscript a denotes approximate pattern. Similar to the development for the sampled aperture pattern, observe that $b^a_{m,n}(u,v)$ and $b^a_{m+1,n}(u,v)$ are related as

$$\left(\frac{2\pi}{\lambda}\Delta_x u - m\frac{2\pi}{N}\right) b^a_{m,n}(u,v) + \left(\frac{2\pi}{\lambda}\Delta_x u - (m+1)\frac{2\pi}{N}\right) b^a_{m+1,n}(u,v) = 0 \tag{59}$$

which may be rearranged as

$$u\,\{b^a_{m,n}(u,v) + b^a_{m+1,n}(u,v)\} = \frac{\lambda}{N\Delta_x}\{m b^a_{m,n}(u,v) + (m+1) b^a_{m+1,n}(u,v)\}. \tag{60}$$

Similarly, $b^a_{m,n}(u,v)$ and $b^a_{m,n+1}(u,v)$ are related as

$$\left(\frac{2\pi}{\lambda}\Delta_y v - n\frac{2\pi}{M}\right) b^a_{m,n}(u,v) + \left(\frac{2\pi}{\lambda}\Delta_y v - (n+1)\frac{2\pi}{M}\right) b^a_{m,n+1}(u,v) = 0 \tag{61}$$

which may be rearranged as

$$v\,\{b^a_{m,n}(u,v) + b^a_{m,n+1}(u,v)\} = \frac{\lambda}{M\Delta_y}\{n b^a_{m,n}(u,v) + (n+1) b^a_{m,n+1}(u,v)\}. \tag{62}$$

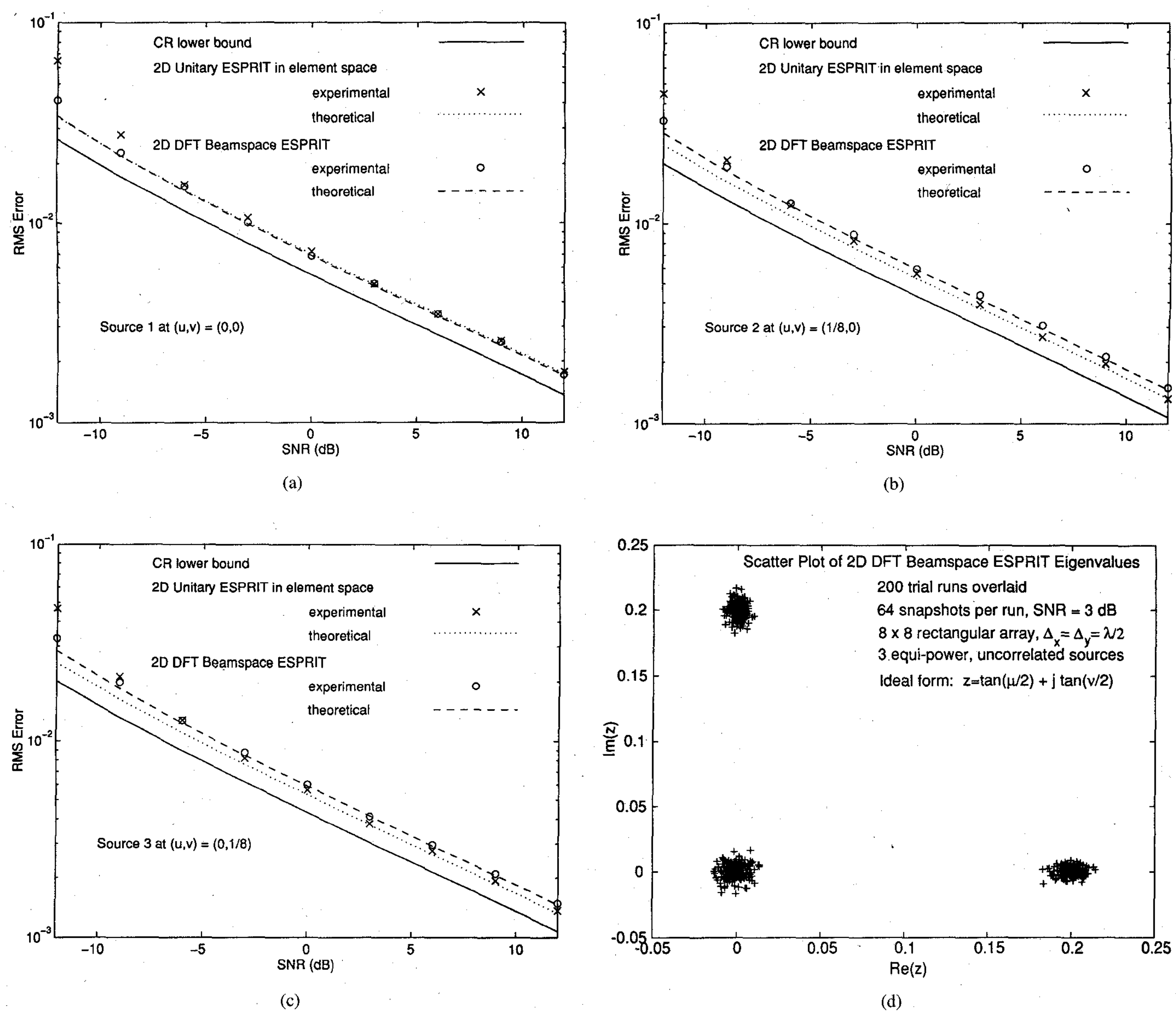

Fig. 4. (a) Performance for source 1 in simulation example; (b) performance for source 2 in simulation example; (c) performance for source 3 in simulation example; (d) scatter plot of 2-D DFT beamspace ESPRIT eigenvalues.

For the sake of brevity, consider again the case of four 2-D DFT beams to estimate the respective azimuth and elevation angles of each of two closely spaced sources. In this case, the 4×1 beamspace manifold is $\mathbf{b}^a(u,v) = [b^a_{m,n}(u,v),\, b^a_{m+1,n}(u,v),\, b^a_{m,n+1}(u,v),\, b^a_{m+1,n+1}(u,v)]^T$. Given the relations above, it is readily deduced that $u\mathbf{\Gamma}^a_{u1}\mathbf{b}^a(u,v) = \mathbf{\Gamma}^a_{u2}\mathbf{b}^a(u,v)$ and $v\mathbf{\Gamma}^a_{v1}\mathbf{b}^a(u,v) = \mathbf{\Gamma}^a_{v2}\mathbf{b}^a(u,v)$, where

$$\mathbf{\Gamma}^a_{u1} = \begin{bmatrix} 1 & 1 & 0 & 0 \\ 0 & 0 & 1 & 1 \end{bmatrix} \quad \text{and}$$
$$\mathbf{\Gamma}^a_{u2} = \frac{\lambda}{N\Delta_x}\begin{bmatrix} m & (m{+}1) & 0 & 0 \\ 0 & 0 & m & (m{+}1) \end{bmatrix}$$

$$\mathbf{\Gamma}^a_{v1} = \begin{bmatrix} 1 & 0 & 1 & 0 \\ 0 & 1 & 0 & 1 \end{bmatrix} \quad \text{and}$$
$$\mathbf{\Gamma}^a_{v2} = \frac{\lambda}{M\Delta_y}\begin{bmatrix} n & 0 & (n{+}1) & 0 \\ 0 & n & 0 & (n{+}1) \end{bmatrix}.$$

Asymptotically, the 4×2 real-valued matrix of signal eigenvectors $\mathbf{E}_S$ satisfies $\mathbf{E}_S = \mathbf{B}\mathbf{T}$ where $\mathbf{B} = [\mathbf{b}(u_1,v_1), \mathbf{b}(u_2,v_2)]$ and $\mathbf{T}$ is an unknown 2×2 *real-valued* matrix. Expediting the development, it follows that $\mathbf{\Gamma}^a_{u1}\mathbf{E}_S\mathbf{\Psi}_u = \mathbf{\Gamma}^a_{u2}\mathbf{E}_S$ where $\mathbf{\Psi}_u = \mathbf{T}^{-1}\mathbf{\Omega}_u\mathbf{T}$ and $\mathbf{\Omega}_u = \text{diag}\{u_1, u_2\}$. Also, $\mathbf{\Gamma}^a_{v1}\mathbf{E}_S\mathbf{\Psi}_v = \mathbf{\Gamma}^a_{v2}\mathbf{E}_S$ where $\mathbf{\Psi}_v = \mathbf{T}^{-1}\mathbf{\Omega}_v\mathbf{T}$ and $\mathbf{\Omega}_v = \text{diag}\{v_1, v_2\}$. Thus, $u_1 + jv_1$ and $u_2 + jv_2$ are the two eigenvalues of $\mathbf{\Psi}_u + j\mathbf{\Psi}_v$.

The point is that with $d \leq \lambda/2$, the sampled aperture pattern is very well approximated by the continuous aperture pattern in the vicinity of the mainlobe and first few sidelobes. Thus, if only a relatively small number of beams is selected, the modified version of *2-D DFT beamspace ESPRIT* sketched above yields the direction cosines directly without spatial warping.

VII. 2-D DFT Beamspace ESPRIT for Cross Array

Consider an array composed of an N element ULA aligned with the x-axis and an M element ULA aligned with the y-axis. The center of each leg is assumed to be at the origin so that they have a common phase center. To ease the development and for the sake of notational simplicity, we will assume M and N are both even so that the two legs do not share a common element at the origin. However, with slight modification, the adaptation of *2-D DFT beamspace ESPRIT* for a cross array developed subsequently may also be employed when M and/or N are odd. Also, due to space limitations, we here only present the appropriate adaptation of *2-D DFT beamspace ESPRIT*. Note that ACMP is not applicable with such an array geometry.

Let $\mathbf{x}(\ell)$ and $\mathbf{y}(\ell)$ be the $N \times 1$ and $M \times 1$ snapshot vectors output by the two respective legs at time ℓ. The $(N+M) \times 1$ composite snapshot vector is formed as $\mathbf{z}(\ell) = \begin{bmatrix} \mathbf{x}(\ell) \\ \mathbf{y}(\ell) \end{bmatrix}$. These are stacked as the columns of an $(N+M) \times N_s$ matrix $\mathbf{Z}$. The array manifold for such an array is

$$\mathbf{a}(\mu, \nu) = \begin{bmatrix} \mathbf{a}_N(\mu) \\ \mathbf{a}_M(\nu) \end{bmatrix} \tag{63}$$

where $\mathbf{a}_N(\mu)$ and $\mathbf{a}_M(\nu)$ are each conjugate centrosymmetric, as defined previously. Note that it is only because the two legs have a common phase center that we are able to express the array manifold in this form. If this is not the case, as with an L-shaped array, for example, either the upper $N \times 1$ or lower $M \times 1$ block of $\mathbf{a}(\mu, \nu)$ would not be conjugate centrosymmetric and it would not be possible to convert $\mathbf{a}(\mu, \nu)$ to a real-valued manifold through a simple matrix transformation.

Transformation to beamspace is accomplished via

$$\mathbf{F} = \begin{bmatrix} \tilde{\mathbf{W}}_N & \mathbf{O} \\ \mathbf{O} & \tilde{\mathbf{W}}_M \end{bmatrix}. \tag{64}$$

The beamspace manifold is

$$\mathbf{b}(\mu, \nu) = \mathbf{F}^H \mathbf{a}(\mu, \nu) = \begin{bmatrix} \mathbf{b}_N(\mu) \\ \mathbf{b}_M(\nu) \end{bmatrix} \tag{65}$$

where $\mathbf{b}_N(\mu)$ and $\mathbf{b}_M(\nu)$ are as defined previously. In practice, transformation to beamspace is accomplished via an N-point DFT of the x-axis leg and an M pt. DFT of the y-axis leg, with *a posteriori* conjugate centrosymmetrization via simple scaling of each DFT value.

Let $\mathbf{E}_S$ be the $(N+M) \times d$ matrix of signal eigenvectors computed as the d "largest" left singular vectors of $[\mathcal{R}e\{\mathbf{H}\}, \mathcal{I}m\{\mathbf{H}\}]$ where $\mathbf{H} = \mathbf{F}^H \mathbf{Z}$. Asymptotically, $\mathbf{E}_S = \mathbf{BT}$ where $\mathbf{B} = [\mathbf{b}(\mu_1, \nu_1), ..., \mathbf{b}(\mu_d, \nu_d)]$ and $\mathbf{T}$ is an unknown $d \times d$ *real-valued* matrix. Define the following matrices:

$$\mathbf{\Delta}_{\mu 1} = [\underbrace{\mathbf{\Gamma}_1}_{N} \vdots \underbrace{\mathbf{O}}_{M}]\,\}N\text{-}1 \quad \text{and} \quad \mathbf{\Delta}_{\mu 2} = [\underbrace{\mathbf{\Gamma}_2}_{N} \vdots \underbrace{\mathbf{O}}_{M}]\,\}N\text{-}1 \tag{66}$$

$$\mathbf{\Delta}_{\nu 1} = [\underbrace{\mathbf{O}}_{N} \vdots \underbrace{\mathbf{\Gamma}_3}_{M}]\,\}M\text{-}1 \quad \text{and} \quad \mathbf{\Delta}_{\nu 2} = [\underbrace{\mathbf{O}}_{N} \vdots \underbrace{\mathbf{\Gamma}_4}_{M}]\,\}M\text{-}1 \tag{67}$$

where $\mathbf{\Gamma}_3$ and $\mathbf{\Gamma}_4$ are defined similar to (25) and (26) with N replaced by M. The following signal eigenvector relations follow quite readily from previous developments:

$$\mathbf{\Delta}_{\mu 1} \mathbf{E}_S \mathbf{\Psi}_\mu = \mathbf{\Delta}_{\mu 2} \mathbf{E}_S \quad \text{where:} \quad \mathbf{\Psi}_\mu = \mathbf{T}^{-1} \mathbf{\Omega}_\mu \mathbf{T} \tag{68}$$

$$\mathbf{\Delta}_{\nu 1} \mathbf{E}_S \mathbf{\Psi}_\nu = \mathbf{\Delta}_{\nu 2} \mathbf{E}_S \quad \text{where:} \quad \mathbf{\Psi}_\nu = \mathbf{T}^{-1} \mathbf{\Omega}_\nu \mathbf{T}. \tag{69}$$

Since all of the quantities in (68) and (69) are real valued, $\mathbf{\Psi}_\mu + j\mathbf{\Psi}_\nu$ may be spectrally decomposed as $\mathbf{\Psi}_\mu + j\mathbf{\Psi}_\nu = \mathbf{T}^{-1}\{\mathbf{\Omega}_\mu + j\mathbf{\Omega}_\nu\}\mathbf{T}$. The algorithm based on these observations is similar in form to *2-D DFT beamspace ESPRIT* for a URA.

VIII. Simulations

Simulations were conducted employing an 8×8 URA (*i.e.*, $N = M = 8$) with $\Delta_x = \Delta_y = \lambda/2$. The source scenario consisted of $d = 3$ equipowered, uncorrelated sources located at $(u_1, v_1) = (0, 0)$, $(u_2, v_2) = (1/8, 0)$, and $(u_3, v_3) = (0, 1/8)$ where u_i and v_i are the direction cosines of the ith source relative to the x and y axes, respectively. Sources 1 and 2 were separated by a half-beamwidth, i.e., half the Rayleigh resolution limit, as were sources 2 and 3. Sources 1 and 2 have the same v coordinate, while sources 2 and 3 have the same u coordinate.

A given trial run at a given SNR level (per source per element) involved $N_s = 64$ snapshots. The noise was *i.i.d.* from element to element and from snapshot to snapshot. The RMS error defined as

$$RMSE_i = \sqrt{E\{(\hat{u}_i - u_i)^2\} + E\{(\hat{v}_i - v_i)^2\}}, \quad i = 1, 2, 3 \tag{70}$$

was employed as the performance metric. Let $(\hat{u}_{i_k}, \hat{v}_{i_k})$ denote the coordinate estimates of the ith source obtained from a particular algorithm at the kth run. Sample RMSE's for both *2-D unitary ESPRIT* and *2-D DFT beamspace ESPRIT* were computed from $K = 500$ independent trials as

$$\widehat{RMSE}_i = \sqrt{\frac{1}{K} \sum_{k=1}^{K} \{(\hat{u}_{i_k} - u_i)^2 + (\hat{v}_{i_k} - v_i)^2\}}, \quad i = 1, 2, 3. \tag{71}$$

The bias of *2-D unitary ESPRIT* for $N_s = 64$ snapshots over the range of SNR's simulated was found to be negligible, as was the bias of *2-D DFT beamspace ESPRIT*. This facilitated comparison with the Cramér–Rao lower bound (CRLB). The CRLB, computed according to formulas provided in [8], and the theoretically predicted performance of both *2-D unitary ESPRIT* and *2-D DFT beamspace ESPRIT*, computed according to formulas provided in [21], are plotted in Figures 4(a), 4(b), and 4(c) for sources 1, 2, and 3, respectively.

The respective RMSE's of *2-D unitary ESPRIT* and *2-D DFT beamspace ESPRIT* for sources 1, 2, and 3 are plotted in Figures 4(a), 4(b), and 4(c), respectively. In accordance with the summary of *2-D unitary ESPRIT* at the end of Section III, the computations required for a single run were as follows:

i) sixty four additions per each of 64 snapshots to transform from complex-valued space to real-valued space

ii) calculation of the three "largest" left singular vectors of a 64×128 real-valued matrix
iii) calculation of the solution to two systems of equations of the form $\mathbf{AX} = \mathbf{B}$, where $\mathbf{A}$ and $\mathbf{B}$ are both 64×3 and real-valued
iv) calculation of the eigenvalues of a 3×3 complex-valued matrix.

The performance of *2-D unitary ESPRIT* is observed to be very close to the CRLB for SNR's greater than or equal to -6 dB, although it does not achieve the CRLB even at the rather high SNR level of 12 dB.

To demonstrate the efficacy of working in a reduced dimension beamspace, *2-D DFT beamspace ESPRIT* employed a 3×3 set of 9 beams with mainlobes rectangularly spaced in the u-v plane and centered at $(u, v) = (0, 0)$. In accordance with the summary of *2-D DFT beamspace ESPRIT* at the end of Section IV, the computations required for a single run were as follows:

i) nine sets of 64 multiplications and 63 additions for each of 64 snapshots to transform from element space to beamspace
ii) calculation of the 3 "largest" left singular vectors of a 9×128 real-valued matrix
iii) calculation of the solution to two systems of equations of the form $\mathbf{AX} = \mathbf{B}$ where $\mathbf{A}$ and $\mathbf{B}$ are both 6×3 and real-valued
iv) calculation of the eigenvalues of a 3×3 complex-valued matrix.

A scatter plot of the three eigenvalues obtained from *2-D DFT beamspace ESPRIT* for each of 200 independent runs at a SNR of 3 dB is displayed in Fig. 4(d). For SNR's greater than or equal to 6 dB, the performance of *2-D DFT beamspace ESPRIT* is observed to be only slightly worse than that of *2-D unitary ESPRIT* despite the dramatic reduction in computational complexity. Similar to *2-D unitary ESPRIT,* there is a gap between the performance of *2-D DFT beamspace ESPRIT* and the CRLB and it is fairly constant as a function of SNR over the range of SNR's simulated (on a logarithmic scale.)

An interesting observation is that for SNR's lower than -6 dB, *2-D DFT beamspace ESPRIT* outperformed *2-D unitary ESPRIT*. This is in accordance with observations made by Xu *et al.* [16] in comparing the performance of their version of *beamspace ESPRIT* with that of *ESPRIT* in element space. At low SNR's, Xu *et al.*. argued that the better performance of the former over that latter is due to fact that *beamspace ESPRIT* exploits *a priori* information on the source locations by forming beams pointed in the general directions of the sources. This argument is applicable here as well.

IX. CONCLUSIONS

2-D unitary ESPRIT is a closed form 2-D angle estimation algorithm for use in conjunction with a URA and is easily adapted for other dual invariance arrays including a cross array. *2-D DFT beamspace ESPRIT* is an efficient beamspace implementation of *2-D unitary ESPRIT* facilitating reduced dimension processing and an attendant reduction in computational complexity. The 2-D angle estimates provided by either *2-D unitary ESPRIT* or *2-D DFT beamspace ESPRIT* may be used as starting points for localized Newton searches of the *2-D MUSIC* spectrum, the ML algorithm, or the *multiple invariance ESPRIT* algorithm. Note that *2-D unitary ESPRIT* may also be employed in a variety of applications other than 2-D angle estimation including 2-D harmonic retrieval for image analysis, for example.

REFERENCES

[1] R. Roy and T. Kailath, "ESPRIT-Estimation of signal parameters via rotational invariance techniques," *IEEE Trans. Acoust., Speech, Signal Processing,* vol. 37, pp. 984–995, July 1989.
[2] A. L. Swindlehurst, B. Ottersten, G. Xu, R. H. Roy, and T. Kailath, "Multiple Invariance ESPRIT," *IEEE Trans. Signal Processing*, vol. 40, pp. 867–881, Apr. 1992.
[3] A. L. Swindlehurst and T. Kailath, "Azimuth/elevation direction finding using regular array geometries," *IEEE Trans. Aerosp. Electron. Syst.*, vol. 29, pp. 145–156, Jan. 1993.
[4] M. P. Clark and L. L. Scharf, "Two-dimensional modal analysis based on maximum likelihood," *IEEE Trans. Signal Processing*, vol. 42, pp. 1443–1452, June 1994.
[5] M. D. Zoltowski and D. Stavrinides, "sensor array signal processing via a procrustes rotations based eigenanalysis of the ESPRIT data pencil," *IEEE Trans. Acoust., Speech, Signal Processing*, vol. 37, pp. 832–861, Jun. 1989.
[6] A. J. van der Veen, P. B. Ober, and E. D. Deprettere, "Azimuth and elevation computation in high resolution DOA estimation," *IEEE Trans. Signal Processing*, vol. 40, pp. 1828–1832, July 1992.
[7] M. D. Zoltowski and C. P. Mathews, "Closed-form 2-D angle estimation with uniform circular arrays via phase mode excitation and ESPRIT," in *27th Asilomar IEEE Conf. Signals, Syst., Comput.*, vol. 1, Nov. 1993, pp. 169–173.
[8] C. P. Mathews and M. D. Zoltowski, "Eigenstructure techniques for 2-D angle estimation with uniform circular arrays," *IEEE Trans. Signal Processing*, vol. 42, pp. 2395–2407, Sept. 1994.
[9] M. Haardt and J. A. Nossek, "unitary ESPRIT: how to obtain increased estimation accuracy with a reduced computational burden," *IEEE Trans. Signal Processing*, vol. 43, pp. 1232–1242, May 1995.
[10] ——, "Unitary ESPRIT: how to obtain increased estimation accuracy with a reduced computational burden," *Tech. Rep. no. TUM-LNS-TR-94-3*, Institute Network Theory Circuit Design, Technical University of Munich, Munich, Germany, May 1994.
[11] K. C. Huarng and C. C. Yeh, "A unitary transformation method for angle-of-arrival estimation," *IEEE Trans. Signal Processing*, vol. 39, pp. 975–977, Apr. 1991.
[12] D. A. Linebarger, R. D. DeGroat, and E. M. Dowling, "Efficient direction finding methods employing forward/backward averaging," *IEEE Trans. Signal Processing*, vol. 42, pp. 2136–2145, Aug. 1994.
[13] K. Buckley and X.-L. Xu, "Spatial-spectrum estimation in a location sector," *IEEE Trans. Acoust., Speech, Signal Processing*,vol. 38, pp. 1842–1852, Nov. 1990.
[14] G. Bienvenu and L. Kopp, "Decreasing high resolution method sensitivity by conventional beamforming preprocessing," in *Proc. 1984 IEEE Int. Conf. Acoust., Speech, Signal Processing*, Apr. 1984, pp. 33.2.1–33.2.4.
[15] H. Lee and M. Wengrovitz, "Resolution threshold of beamspace MUSIC for two closely-spaced emitters," *IEEE Trans. Acoust., Speech, Signal Processing*, vol. 38, pp. 1545–1559, Sept. 1990.
[16] G. Xu, S. D. Silverstein, R. H. Roy, and T. Kailath, "beamspace ESPRIT," *IEEE Trans. Signal Processing*, vol. 42, pp. 349–356, Feb. 1994.
[17] M. D. Zoltowski, G. M. Kautz, and S. D. Silverstein, "Beamspace root-MUSIC," *IEEE Trans. Signal Processing*, vol. 41, pp. 344–364, Jan. 1993.
[18] G. Xu, R. H. Roy, and T. Kailath, "Detection of number of sources via exploitation of centro-symmetry Property," *IEEE Trans. Signal Processing*, vol. 42, pp. 102–112, Jan. 1994.
[19] M. D. Zoltowski and T. Lee, "Maximum likelihood based sensor array signal processing in the beamspace domain for low-angle radar tracking," *IEEE Trans. Signal Processing*, vol. 39, pp. 656–671, Mar. 1991.

[20] F. Vanpoucke, M. Moonen, and Y. Berthoumieu, "An efficient subspace algorithm for 2-D harmonic retrieval," in *Proc. IEEE Int. Conf. Acoust., Speech, Signal Processing*, Adelaide, Australia, Apr. 1994.
[21] C. P. Mathews, M. Haardt, and M. D. Zoltowski, "Implementation and Performance Analysis of 2-D DFT beamspace ESPRIT," to be presented at and included in *Conf. Rec. 29th Asilomar IEEE Conf. Signals, Syst., Comput.*, Oct.–Nov. 1995.

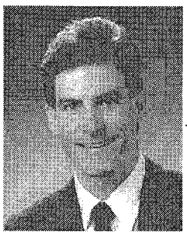

Michael D. Zoltowski (S'80–M'86–SM'95) was born in Philadelphia, PA, on August 12, 1960. He received both the B.S. and M.S. degrees in electrical engineering with highest honors from Drexel University, Philadelphia, PA, in 1983 and the Ph.D. degree in systems engineering from the University of Pennsylvania in 1986.

From 1982 to 1986, he was an Office of Naval Research Graduate Fellow. In Fall 1986, he joined the faculty of Purdue University, West Lafayette, IN, where he currently holds the position of associate professor of electrical engineering. He has also served as a consultant to the General Electric Company. As associate professor, he was the recipient of the IEEE Outstanding Branch Counselor Award for 1989-1990 and the Ruth and Joel Spira Outstanding Teacher Award for 1990–1991. During 1987, he was a Summer Faculty Research Fellow at the Naval Ocean Systems Center in San Diego, CA. he received the IEEE Signal Processing Society's 1991 Paper Award (Statistical Signal and Array Processing Technical Area). He is a contributing author to *Adaptive Radar Detection and Estimation* (Wiley, 1991), and *Advances in Spectrum Analysis and Array Processing, Vol. III* (Prentice-Hall, 1994). He is presently an associate editor for the IEEE TRANSACTIONS ON SIGNAL PROCESSING, and a member of the Technical Committee for the Statistical Signal and Array Processing Area of the Signal Processing Society. His current research interests include antenna array processing and blind adaptive beamforming for mobile communications, GPS, and radar.

Martin Haardt (S'90) was born in Germany on October 4, 1967, and received the D.I. degree in electrical engineering from the Ruhr University Bochum, Germany, in 1991.

From 1989 to 1990, he was a visiting scholar at Purdue University, West Lafayette, IN, sponsored by a fellowship of the German Academic Exchange Service (DAAD). From 1991 to 1993, he worked for Siemens AG, Corporate Research and Development, in Munich, Germany, conducting research in the areas of image processing and biomedical signal processing. Since 1993 he has been a research associate with the Institute of Network Theory and Circuit Design at the Technical University of Munich, Germany, where he is also working toward the Ph.D. degree. His current research interests include array signal processing, spectral estimation, numerical linear algebra, and mobile communications.

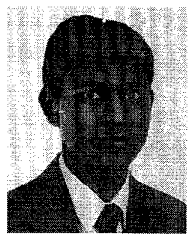

Cherian P. Mathews was born in Madras, India, in 1966. He received the B.E. degree in electrical and electronics engineering from Anna University, Madras, in 1987, and the M.S. and Ph.D. degrees in electrical engineering from Purdue University, West Lafayette, IN, in 1989 and 1993, respectively.

He served as a visiting assistant professor at Purdue University between January and May 1994, and at Rose-Hulman Institute of Technology, Terre Haute, IN, between August 1994 and July 1995. Since July 1995, he has been with the Department of Electrical Engineering at the University of West Florida, Pensacola, FL, USA, where he is currently an assistant professor. His current research interests are in sensor array signal processing for radar and mobile communications. He is a contributing author to *Advances in Spectrum Analysis and Array Processing, Vol. III* (Prentice-Hall, 1995).